# Advances in processing and application of high temperature superconducting coated conductors

*Judith L MacManus-Driscoll [1,*] and Stuart C Wimbush [2]*

[1] Department of Materials Science & Metallurgy, University of Cambridge, 27 Charles Babbage Road, Cambridge CB3 0FS, United Kingdom.

[2] Robinson Research Institute, Victoria University of Wellington, PO Box 600, Wellington 6140, New Zealand.

[*] e-mail: jld35@cam.ac.uk

Abstract | $REBa_2Cu_3O_{7-\delta}$ (REBCO, where RE is a rare earth element) high temperature superconducting (HTS) materials in the form of coated conductors offer energy-efficient, high power density delivery of electricity making them essential components of clean energy generation, conversion, transmission and storage systems. HTS materials of this type have now been researched for more than 30 years and multi-$bn have been invested across government and industry with the goal of achieving practical coated conductor wires in kilometre lengths with high performance (high current-carrying capacity from low to high magnetic field) at low cost. Two challenges remain: improving the wire performance in order to operate at as high a temperature as possible under a given magnetic field, and even more importantly, lowering the cost of the wire to enable broader applications uptake. Here we review the status of HTS coated conductor processing and applications. First, we compare contemporary commercially sourced conductor wires, and then we assess recent advances in laboratory-scale conductors with commercial potential. We show that the nature of the resulting materials' nanostructures and the consequent wire performance across different applications regimes are related to the inherent supersaturation levels of the different processing methods employed in production. Subsequently, we outline ways to lower wire cost and improve wire performance in the most critical applications regime, from 20 K to 40 K in temperature and above 1 T in magnetic field. Finally, emerging applications that are reliant upon HTS coated conductors and may therefore break the cost-demand cycle are briefly discussed.

## 1 History of HTS wire development

Since the discovery of high temperature superconductivity[1] at above liquid nitrogen temperature[2] in the cuprates in the late 1980s, there have been enormous efforts to create practical superconductors that meet industry needs, and to do this at sufficiently low cost for the resulting applications to be economically viable. At the same time, as the technology has progressed, a rich understanding of the physics of these exotic, quasi two-dimensional materials has been gained, hugely benefitting the broader field of strongly correlated oxides that has emerged in parallel. Numerous cuprate superconductors have been identified, having critical temperatures ranging up to 135 K at ambient pressure,[3] but for reasons of either poor tolerance to applied magnetic fields, high toxicity, or excessively complex processing routes, only the Bi-based cuprates (Bi-2223 and Bi-2212) and the rare-earth based cuprates (RE-123 or REBCO) are of present technological interest.[4] At low enough temperatures, the Bi-based cuprates perform sufficiently well in field and owing to the mature manufacturing process of Bi-2223, its steady improvement in properties over time,[5] consistency, predictability[6] and availability of supply, they have been and continue to be used for high field magnet applications.[7,8] However, greater performance at lower cost remains necessary for broader application, and REBCO conductors offer the promise of being able to be operated at more accessible temperatures or in the generation of still higher magnetic fields.[9,10,11,12,13,14] That said, after 30 years of intensive worldwide effort and enormous financial investment, challenges in this area remain. This is not surprising.

Comparing superconductors with other functional materials (e.g. semiconductors, ferroelectrics, dielectrics and magnetics), the vastly greater complexity is apparent: they require simultaneous high precision engineered perfection and imperfection, rather than simple perfection as in the other cases. By way of comparison, it took almost 50 years from the first demonstration of semiconductor rectification for detecting radio waves by Bose to the invention of the semiconductor transistor by Bardeen and Brattain,[15] and this technology involves a comparatively simple elemental material. Even comparing against the technological low-temperature superconductors, it is instructive to note that it took 30 years of development to bring Nb–Ti, a binary metallic alloy, up to a production capacity of 20,000 km per year at a pricing level of $1 per kAm (when operated at 4.2 K), driven by the mass uptake of magnetic resonance imaging (MRI) technology.[16] REBCO, in contrast, is neither an elemental material nor a simple alloy but rather a quaternary system with variable oxygen stoichiometry having a decisive impact on its functional properties, which are also strongly anisotropic and highly correlated. Furthermore, its physical properties are complex with its high critical temperature being concomitant with a low superconducting coherence length, causing grain boundaries within the material to form weak links and requiring flux pinning defects to be of nanoscale size and distribution to be effective. The 2D nature of the superconducting planes also causes complications as it makes electronic transport perpendicular to the planes poor and requires very high grain alignment in the material to permit current to be transferred without obstruction along the length of a conductor. Finally, targeted nanoscale pinning defects need to be engineered into the material without disrupting the superconducting planes or causing blocking of supercurrent transport through the grain boundaries. To achieve the required grain alignment and nanoscale defect microstructure, REBCO conductors must be manufactured by epitaxial thin film growth methods. Also, the conductor tapes must be long and flexible to facilitate application. Consequently, brittle, epitaxial REBCO films must be deposited on a lengthy, flexible metallic substrate which is a complex and ultimately costly process.

The intention of this review is to take an overarching look at REBCO conductors, comparing the performance of highly validated industrially-produced wires prepared using different processing methods, explaining the underlying reasons for the different performance profiles achieved, listing the unknowns, highlighting new approaches which show the potential for performance enhancements over standard industry methods, and proposing new ways to improve future performance at an acceptable cost. Even after 30 years of effort, there is new understanding to be gained and unexplored directions to be followed. Within this timeframe also, the climate emergency has become very real, and with it has grown the need for new energy-efficient power devices if we are to mitigate the worst of its effects whilst maintaining our energy-intensive technologically advanced lifestyles. Superconductivity is a key enabling technology in this area and it is therefore imperative that new science capable of meeting the performance and cost challenges be pursued.

Before discussing the different processing methods used to produce coated conductors and the different performance profiles that stem from each, we briefly consider the crucial energy-related applications that could be enabled by the development of cost-effective high-performance REBCO coated conductors.[17] We then return to discussing emerging applications towards the end of the review. The range of potential applications of HTS promising a step change in efficiency, performance and/or functionality is vast – essentially all aspects of power infrastructure from generation through distribution and grid resilience to consumption, including transportation in all forms from personal vehicles through mass transit to shipping, aircraft and beyond to space travel.[18] Many of these applications have already been demonstrated in principle and several are now being actively developed for commercial implementation, as illustrated in the timeline of Fig. 1. Examples include power cables, fault current limiters, transformers, wind turbine and other generators, magnetic energy storage devices, motors for transportation including marine propulsion systems and magnetic levitation systems for trains.[19] Beyond the energy sector lie other applications in high-field magnets for medical applications such as MRI[20] and ion[21] or proton[22] therapy, research applications such as

NMR spectroscopy[23] and accelerator magnets,[24] and other purposes such as induction heaters[25] and current leads[26] or busbars.[27]

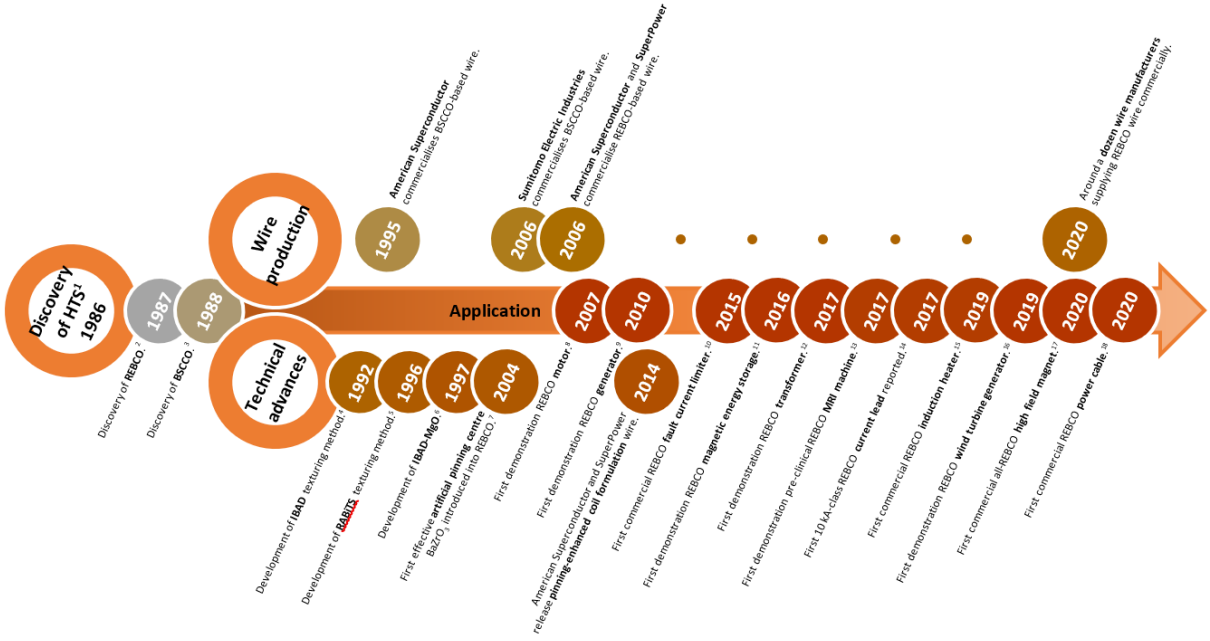


Fig. 1 | **Timeline of significant events in the development of HTS coated conductors for application.**

## 2 Applications performance requirements

Fig. 2a plots the critical surface for a typical REBCO wire, showing the maximum current ($I_c$) that can be carried per unit width of wire ($w$) at different temperatures ($T$) and magnetic fields ($B$), applied in the conventionally least favourable direction perpendicular to the superconducting planes (parallel to the crystallographic $c$ axis of the superconductor). $I_c$ falls steeply with field (plotted here on a logarithmic scale) and somewhat more gradually with temperature from its peak value at 0 K and zero field. This decay in $I_c$ highlights a key detriment of HTS materials: their inability to carry high current near their critical temperature in moderate fields due to the positive curvature of the irreversibility line. Obviously, to minimise the cooling burden and to potentially make use of simple and cheap cryogenic cooling systems based on liquid nitrogen, it would be desirable to operate at 77 K, but for most applications, the required level of in-field performance cannot be attained because it has not proved possible to adequately pin the magnetic flux vortices against the action of the Lorentz force resulting from the electromagnetic interaction of current and field. Consequently, lower operating temperatures are required to provide deeper pinning potentials through the increased condensation energy of the superconductor.

The regions within the $I_c$-$T$-$B$ space where key applications lie are shown. Where applications requirements fall above the critical surface, presently available conductor performance is inadequate. For many applications, use of cryogen-free electrical refrigeration to 20–40 K is both practical and acceptable, enabled by the simultaneous steady development of cryocooler technology in terms of both performance and reliability over the last 30 years.[28] Cryocooler efficiencies are greater at higher temperatures, and this is compounded by the underlying Carnot efficiency which also drops off towards lower temperatures. So, while at 77 K, the Carnot efficiency is 3 W/W (3 W of input power required to give 1 W of cooling power) and a modern cryocooler may have an efficiency exceeding 10–15% of Carnot, at 4.2 K the Carnot efficiency drops to 70 W/W and cryocooler efficiencies may be as low as 1% of Carnot.[29] In practice, this means that mid-scale practical applications can presently be adequately cooled using electrical cooling down to around 20 K, although these efficiencies are improving all the time. As with the superconducting wire itself, increasing

application demand can be expected to lead to further improvements in cryocooler technology as well as a reduction in the associated cost.

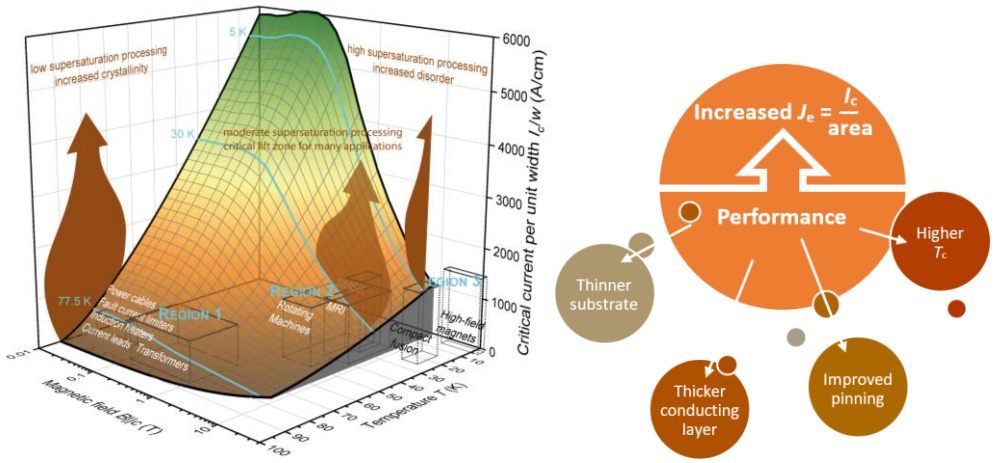


Fig. 2 | **Critical surface diagram and routes to improving conductor performance. a** | Critical surface of a typical commercial REBCO conductor with regions of common application of high temperature superconductors and performance requirements outlined. The material is superconducting only below the surface. The central region, **REGION 2**, is where most potential HTS applications lie, and where new opportunities for performance optimisation exist. **b** | Routes to improving the performance of coated conductor wires (expressed in terms of the engineering critical current density, $J_e$, which is the $I_c$ divided by the total cross-sectional area of the conductor). The effect of these improvements is to push the critical surface upwards, as indicated by the brown arrows on part (a).

Below, we identify the three distinct regions labelled on Fig. 2a within which the main applications lie and describe briefly the nature of the defects and the form of the processing which benefits each, summarising how $I_c$ is optimised under the different conditions. We include how the inherent supersaturation of the process (the concentration of the REBCO chemical species which is above the equilibrium level and thereby drives the nucleation – high supersaturation resulting in increased nucleation and therefore finer crystallites) is suited to the different regions, and the potential ways of increasing $I_c$ (with reference to Fig. 2b). Later, we discuss further details of the supersaturation of the different processes and how this influences microstructure and vortex pinning.

**REGION 1A**: 65–77 K, self-field (< 0.1 T). Here, the performance of industrial conductors is highly optimised. To achieve high $I_c$ at 77 K and self-field, highly perfect, highly aligned grains with few pinning defects are required. The critical temperature should be kept as close as possible to its maximum value of 92–95 K (dependent on the rare earth constituent) as small reductions have a relatively large effect on performance at high temperature. Low supersaturation processing is ideal for this region. Thicker films are more challenging to produce by lower supersaturation methods and hence there is a natural limitation to the achievable $I_c$.

**REGION 1B**: 65–77K, 0.1–1 T. This region is desirable for transformers, which typically operate in liquid nitrogen both for cost-effectiveness and as a substitute for the oil that is commonly used as a dielectric and coolant in conventional transformers. It is the most challenging region as the high degree of thermal activation at the elevated temperature makes effective pinning difficult, particularly as the field strength increases.

**REGION 2:** 20–40 K, > 1 T. This region is critical for many important applications, but historically less attention has been directed to this temperature regime. Achieving high critical currents that can be sustained in high magnetic fields at operating temperatures of 20 K and above is challenging. A complex defect landscape is required as well as greater understanding about both the optimal nature of this landscape and how to engineer it effectively. Later, we show that moderate supersaturation processing is ideal for this region.

**REGION 3:** up to 10 K, above 10 T. This region encompasses high-field magnet applications. Current wire performance is exceptional here, with commercial conductors already able to exceed 1000 A cm$^{-1}$ at 4.2 K,

10 T, and laboratory-scale conductors indicating significant improvement potential – a factor two or more – over this. A high density of very fine point defects is required to adequately pin the high number of flux lines resulting from the high field. High supersaturation processing is ideal for this region.

# 3 Coated conductor architecture and cost

The complexity of the coated conductor architecture (Fig. 3a) is remarkably high compared to other industrial materials in use today, whether they be for electronics (e.g. Si-based, organic) or for power and magnetic applications (mainly metallic alloys). At the same time, the superconducting material itself, a complex quaternary oxide, is arguably one of the most chemically advanced materials in industrial production today. Adding to this the requirement for conductor flexibility, and the need for shunting, strengthening and insulating layers and post-engineering of the conductors, it is clear that much new thinking and great innovation has been brought to bear on the successful manufacture of high-performance coated conductors.

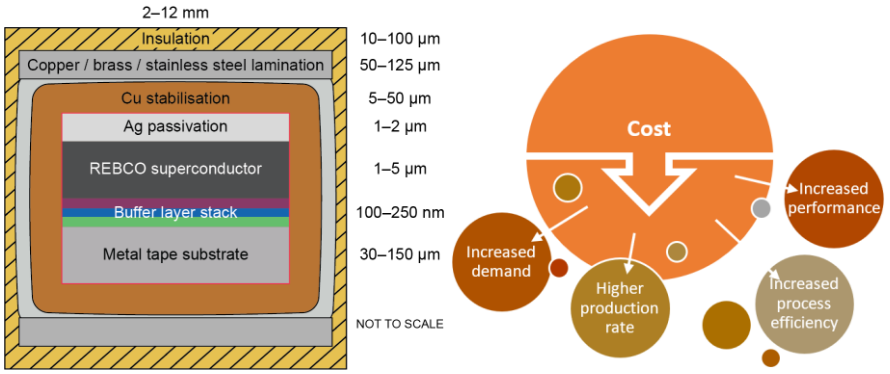


| Texturing method | IBAD | RABiTS |
|---|---|---|
| **Advantages** | Thinner buffer layers<br>Improved texture<br>Wider substrate choice | Non-vacuum process possible<br>Large areas possible |
| **Disadvantages** | Vacuum process required<br>Large areas challenging | Careful heat treatment required<br>Magnetic substrate (typically)<br>Poorer texture<br>Lengthy processing |

Fig. 3 | **Coated conductor architecture, routes to reducing conductor cost, and comparison of texturing methods. a** | A generic coated conductor architecture, highlighting the functional elements. In all cases, a metal tape substrate is rendered suitable to support the growth of a highly textured, biaxially aligned REBCO superconductor layer, aided by the deposition of a stack of intermediary buffer layers providing planarization, passivation and texturing as required. The superconductor is protected from the environment through a silver passivation layer, and a copper coating serves as electrical stabilisation. A laminate is often used to afford increased mechanical strength to the conductor, which may be insulated from its neighbours via a paper or polyimide wrap or coating. **b** | Routes to lowering the cost of coated conductor wires. Here, production rate combines throughput and yield, process efficiency includes such factors as lower-vacuum processes and simpler wire architectures, while the possibility of lowering cost through increasing performance (Fig. 2b) is also recognised. **c** | Advantages and disadvantages of the ion beam assisted deposition (IBAD) and rolling assisted biaxially textured substrates (RABiTS) methods used to achieve an epitaxial REBCO layer.

The coated conductor architecture has been developed over many years, some steps through trial and error, others by extensive research and still others cross-adopted from other fields. There are an increasing number of commercial suppliers around the world (around a dozen at present) involved in manufacturing coated conductors. Each of the different layers in the stack has a specific purpose and a range of processing methods are needed to fabricate them all, many involving state-of-the-art thin film deposition methodologies which we do not attempt to describe in detail here. However, a key aspect to emphasise is the two different types of substrate used to generate biaxial alignment of the superconducting film, either ion beam assisted deposition (IBAD)[30] of a biaxially aligned buffer layer onto an untextured substrate, or a rolling assisted biaxially textured substrate (RABiTS).[31] Each substrate has its advantages and disadvantages (Fig. 3c). In the IBAD process, an oxide layer, nowadays almost universally MgO due to its rapid processing,[32] is deposited onto a polycrystalline non-magnetic alloy of Ni such as Hastelloy or a stainless steel metal substrate under

the simultaneous action of an ion beam which induces a biaxial texture in the growing layer through orientationally-selective etching. Variations of the IBAD process include alternating beam assisted deposition (ABAD)[33] in which the deposition and etching processes are alternated rather than simultaneous and inclined substrate deposition (ISD)[34] in which the biaxial texture is achieved through the fast, anisotropic growth and self-shadowing of the deposited material itself. Subsequent growth of the REBCO layer achieves a 2°–3° average grain misorientation, comparable to what is achieved by growing on single crystal substrates. Vapour deposition is inherent to the IBAD process and is typically also used for the other buffers and the REBCO layer when this method is adopted.[35] For RABiTS, the substrate (a Ni–W alloy) is rolled to induce a biaxial texture with a 5°–7° average grain misorientation. The subsequent buffer layers can either be vapour deposited[36] or solution deposited.[37] The REBCO layer is always solution deposited in this case, followed by thermal processing to crystallise and biaxially texture the grains. Solution deposition is better suited to RABiTS because the heat treatment to form the REBCO grains leads to large meandering grain boundaries.[38] Such meandered grains can accommodate higher angle grain boundaries for high current flow and thereby overcome the poorer substrate texture compared to IBAD.

For many applications, particularly those involving magnet coils, the parameter of overriding importance is the critical current averaged across the entire conductor cross-section. This so-called "engineering" critical current density, $J_e$, depends not only on the actual critical current density of the few micrometre thick REBCO layer but also on the overall architecture of the conductor. Doubling the thickness of the superconducting layer or doubling the critical current density of the superconductor will directly double $J_e$. But the same practical performance enhancement can also be achieved by halving the overall conductor thickness, giving consideration to substrate, stabiliser, laminate and insulation. This opportunity for significant performance gains has driven efforts to reduce substrate thickness, which has seen the former standard of 100 µm drop to 30 µm[39] and even less.[40] This capability has not yet, however, been reported for RABiTS substrates.

In addition to performance, cost is a vital consideration for widespread coated conductor deployment. It should be noted, however, that for some niche applications cost is not a key concern. These applications can only use HTS to give the required performance, and so the technology does not have to compete against established conventional alternatives. Cost is normalised by performance and can be reduced by increasing demand, production rate or process efficiency (Fig. 3b). Today, conductors of more than 100 m piece length are manufactured at rates exceeding 1000 km per yr annual global production. However, the cost remains too high (around or above $100 per kAm) for widespread uptake. If production rate were increased by an order of magnitude, the cost could drop below $10 per kAm[41] which would give a conductor half the price of copper, and equal to the cost of $Nb_3Sn$ operating at 4.2 K. This rate of production is the product of the raw throughput of the process together with the yield. (Manufacturers don't report their yield, but it is anticipated to be around 80% in the best case.) Process efficiency depends on the choice of process and the architecture of the wire. The route to decreasing architecture complexity is not straightforward and is not addressed further here.

# 4 The different REBCO processing methods

As shown in Table 1, many different processing methods exist for making high quality REBCO conductors, each having different features, notably whether they involve *in situ* or *ex situ* REBCO formation, vacuum processing, liquids and line-of-sight deposition, as well as their relative throughput and typical maximum layer thicknesses. Above the Table, we show schematic cross-sections of REBCO containing artificial pinning centres and intrinsic defects, and show relative grain sizes, as well as the defect types, dimensions and densities typically present. We discuss the reason for the different microstructural forms and their relation to the in-field current carrying performance later. At the bottom of the Table, we qualify the potential for

performance improvements in **REGION 2** where many important applications lie and again we discuss this in more detail later.

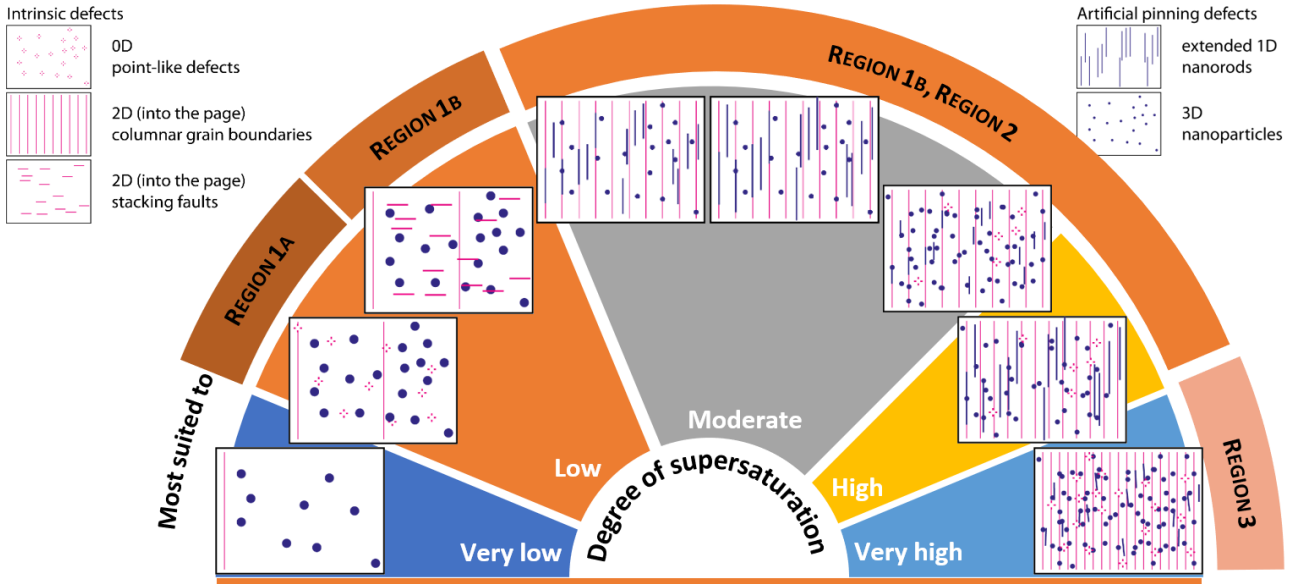


| | LPE | RCE-DR (e-beam) | CSD | RCE-CDR (thermal) | MOCVD | High rate PLD + liquid | Standard PLD | High rate PLD |
|---|---|---|---|---|---|---|---|---|
| REBCO formation | *In situ* | *Ex situ* | | *In situ* | | | | |
| Vacuum process | ✗ | ✓ | ✗ | ✓ | ✓ | ✓ | ✓ | ✓ |
| Liquid-based | ✓ | ✓ | ✓ | ✗ | ✗ | ✓ | ✗ | ✗ |
| Commercialised | ✗ | ✓ | ✓ | ✓ | ✓ | ✗ | ✓ | ✓ |
| Throughput | +++ | +++ | ++ | ++ | ++ | +++ | ++ | +++ |
| Typical maximum REBCO thickness | ~ 3 µm | ~ 2 µm | ~ 1 µm | ~ 3 µm | ~ 3 µm | ~ 5 µm | ~ 5 µm | ~ 5 µm |
| Potential for **REGION 2** improvement | – | ++/+++ | +/++ | +++ | +++ | +++ | + | + |
| | | Non line-of-sight | | Line-of-sight | | | | |

Table 1 | **The different processing methods used in the production of the superconducting layer of HTS coated conductors, and the defect structures that result.** A range of correlated and uncorrelated defects (nanorods, grain boundaries, stacking faults, nanoparticles, and associated strained regions around defects) are present in varying amounts, dimension and spacing for each method. The blue vertical lines represent correlated defects (nanoparticles from the addition of artificial pinning additives, which self-assemble into nanorods) while the red vertical lines indicate columnar grain boundaries. The density of these correlated defects increases with increasing supersaturation and is much higher for line-of-sight methods. Blue circles represent uncorrelated nanoparticle pinning centres and red stars uncorrelated 0D defects. In general, larger and less correlated pinning centres are formed for the non line-of-sight growth methods or when growth kinetics are limited (high rate, low temperature). The red horizontal lines indicate stacking faults that are particularly prevalent in CSD films.

From right to left, i.e. from highest to lowest degree of supersaturation, the different methods are:

- pulsed laser deposition (PLD),[42] where we distinguish a high rate growth > 0.2 µm min$^{-1}$ from the more standard *ca.* 0.1 µm min$^{-1}$.[43] We also include the non-commercial high rate PLD + liquid process because it is a straightforward modification of PLD with the potential to yield thick films with similar performance to PLD but at higher growth rates;
- metal organic chemical vapour deposition (MOCVD),[44] in which a precursor gas mixture undergoes pyrolysis before adsorbing onto the substrate surface and reacting to form REBCO;
- reactive co-evaporation: cyclic deposition and reaction (RCE-CDR)[45] which involves the thermal evaporation of metal oxide precursors with *in situ* reaction[46] at elevated temperatures;

- chemical solution deposition (CSD)[47] which involves slot die coating of a metal organic precursor followed by a post-reaction *ex situ* heat treatment to crystallise the REBCO;
- reactive co-evaporation: deposition and reaction (RCE-DR)[48] which involves the electron beam evaporation of amorphous metal precursors in a reactive atmosphere to form oxides that are deposited at low temperatures followed by *ex situ* reaction to form REBCO by rapidly increasing the oxygen partial pressure at elevated temperatures, via a liquid phase reaction;
- liquid phase epitaxy (LPE)[49] which involves growing REBCO from a melt. LPE enables very rapid growth of highly crystalline REBCO with good self-field values at 77K. While it is not practical for commercial use owing to the need for high temperature growth and the use of a chemically aggressive melt, as the lowest supersaturation process it serves to complete the picture of how REBCO performance is related to the degree of supersaturation, all other factors being equal (e.g. same level of pinning additions).

We order the different methods in sequence of increasing supersaturation since this reflects the thermodynamic driving force influencing the film microstructure, both the intrinsic microstructure arising from the growth process and the extrinsic microstructure arising from artificial pinning centre additives. Even though the growth methods used for coated conductors can be very different – for example, growth of REBCO from an amorphous precursor via a liquid (RCE-DR) is very different to growth from a chemical vapour phase (MOCVD) – the same principles of nucleation and growth apply, i.e. how easy it is to nucleate the REBCO and how fast and in what direction the grains grow. These factors depend on supersaturation, and on the kinetics and directionality of the growth process.

For the case of coated conductors where artificial pinning centres are added or where inclusions form from the components of the REBCO itself (e.g. $RE_2O_3$), the supersaturation is directly applicable only to the majority phase, i.e. the REBCO phase which nucleates heteroepitaxially on the top buffer layer and forms the film matrix. The nucleation density of the REBCO grains depends closely on the supersaturation of the REBCO species.[49] The inclusions, on the other hand, are of low concentration relative to the REBCO (typically <10% of the film) and so supersaturation is not directly relevant to their growth. However, there is an indirect link between supersaturation and the kinetics of film growth[50] and hence to the microstructure of the inclusions. For example, for PLD if the repetition rate of the laser is high, the supersaturation of the REBCO will be high (a high concentration of vapour species is delivered to the substrate surface), but then the film growth rate is also high. This means that there is insufficient time for the inclusion material to diffuse within the film to find another inclusion to nucleate on. The inclusions then nucleate and grow as isolated 3D nanoparticles[50] instead of extended 1D nanorods.[51]

Coated conductor performance in the different regions of the $I_c$-*T*-*B* space has not previously been linked to the degree of supersaturation of the growth method, and yet this provides important insight necessary for comparing and understanding current wire performance, and also for devising new ways to achieve further performance improvements.

In Fig. 4, we show each processing method on a generic diagram plotting degree of supersaturation against crystallographic lattice misfit with the upper buffer surface on which the REBCO is grown. Most buffer misfits lie around 0.5–2% and hence, except for LPE, the processes typically involve 3D nucleation. High supersaturation is achieved by having a high concentration influx of precursors during growth.[52] This is the case for PLD where a large amount of material is ablated rapidly with each laser pulse. It is very low for LPE where the rare earth content is low in the liquid phase. Columnar growth following 3D nucleation is ensured by the line-of-sight processes.[53] Here, a constant flux of material is delivered normal to the substrate. As we discuss later, defects associated with columnar grain boundaries are effective pinning centres in **REGIONS 2 and 3**. In the following sections, we summarise the merits of the high, moderate and low supersaturation processes for the different operating regions.

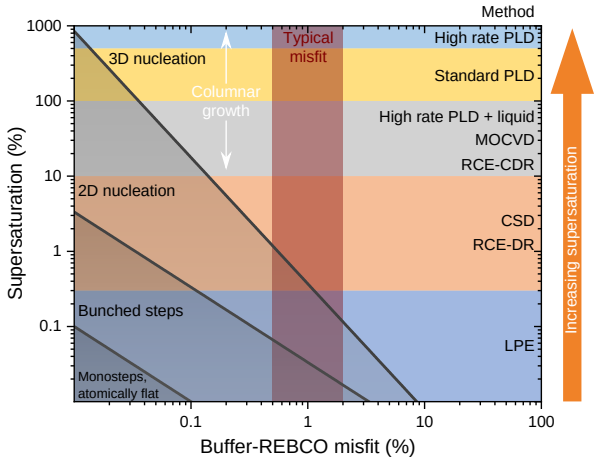


Fig. 4 | **Growth mode resulting from different supersaturation processing methods and crystallographic misfit.** 3D nucleation and columnar growth is the preferred growth mode for producing REBCO coated conductors with strong pinning in **Regions 2 and 3**. Figure adapted from [54].

## 4.1 High supersaturation methods

The key advantages of the high supersaturation methods (standard and high rate PLD) are:

1) Production of more disordered material owing to the fast delivery of highly energetic atomic species and consequently fast growth inducing a high density of 3D nuclei, as well as disorder associated with the fine columnar grains.[55] A wide-ranging defect pinning structure is achieved while still creating highly epitaxial films. Grain alignment is not compromised by the fast growth owing to the strong driving force for vertical growth. For high field pinning in **Region 3**, the very high supersaturation process (high rate PLD) is ideal.

2) Formation of very fine, highly columnar grains. This means that at lower temperatures there can be pinning from the grain boundaries and associated dislocations,[56,57,58,59] which is particularly effective in **Regions 2 and 3**.

3) Ability to deposit thicker films (> 2 µm)[60] because homogenous nucleation of misaligned material is less likely with a high supersaturation columnar growth process. Also, since the 3D nucleation regime extends over a wide range of supersaturation, reproducible microstructures are achieved over a wider range of processing conditions than is the case for low supersaturation methods, i.e. there are less rigid constraints on the growth conditions, precursor composition and substrate condition. This is important in **Regions 1b, 2 and 3**. It is also important for commercial production of coated conductors where process uniformity is critical.

The key disadvantage of the high supersaturation methods is that they require vacuum deposition. Combined with the requirement for laser ablation to achieve the highest degree of supersaturation, this results in the costs of both plant and operation being relatively high. Although laser costs have been steadily reducing, and their reliability and operational characteristics have recently been greatly enhanced, the overall process cost and complexity still cannot compete with the chemical methods. That said, these factors are no longer the barrier to commercial operation that they used to be and the wide-ranging advantages listed above have meant that PLD has become more popular in recent years, particularly for those applications where low cost is not as important as high performance and reproducibility.

## 4.2 Moderate supersaturation methods

While the moderate supersaturation methods RCE-CDR and MOCVD do not offer the full advantages of the high supersaturation methods – their process windows are narrower and there may be more limitations on film thickness – the performance of industry conductors is generally as good as PLD conductors, with the

possible exception of **REGION 3**. Another moderate supersaturation method that is emerging is high-rate PLD + liquid.[61] As shown in Table 1, this method lies between MOCVD and standard PLD in terms of supersaturation, and hence it should be applicable across **REGIONS 1B, 2 and 3.** We discuss this method briefly in section 6.1.

### 4.3 Low supersaturation methods

A key advantage of the low supersaturation methods is that they don't necessarily require vacuum; CSD does not, although RCE-DR does. The REBCO is formed by post-deposition reaction. As shown in Fig. 4, in the absence of a moderate substrate misfit, 2D nucleation would prevail. In general for line-of-sight (*in situ*) methods there is a driving force for columnar growth but in non line-of-sight (*ex situ*) methods such as CSD, there is not and the resulting grains have a strong planar character.[62] In an exception to this general rule, the RCE-DR process does have a moderate driving force for columnar growth owing to large oxygen gradients perpendicular to the surface of the growing film which act to drive grain growth in this direction. However, there is also a driving force for lateral growth because the fast growth direction of REBCO is the *ab*-direction and the presence of liquids promotes lateral growth, so a hybrid grain structure results.[63]

Low supersaturation methods are very well suited to **REGION 1** applications. CSD uses solution precursors which are reacted post-deposition. Making high performance films much thicker than 1 μm without complex layering and prolonged heat treatments is challenging.[64] This is because random homogeneous nucleation is more likely for the lower supersaturation methods, particularly for CSD where the reaction process of the precursors is very complex.[65] Hence, slower growth rates are needed to give a controlled reaction, and to prevent random nucleation of misoriented grains. Such slow reactions mean that pinning centres coarsen during the reaction. Hence pinning particles are typically larger than in PLD growth and the pinning at higher fields is less effective. That said, liquid additions to the reaction step have recently been demonstrated with CSD, enabling greater speed of growth.[66]

While the RCE-DR method is also a low supersaturation method, in practical-thickness films (~2 μm), it gives similar pinning performance to CSD at much higher REBCO growth rates; up to 6 μm $min^{-1}$ for RCE-DR[67] compared to 10–30 nm $min^{-1}$ for CSD,[68] hence over 200 times faster. This is because the reaction is much simpler both chemically (no organic materials or fluorine present) and mechanistically (a liquid layer is continuously present and resides on the surface of the growing film, rather than being transient and disposed throughout the film). However, while the RCE-DR REBCO growth rate is extremely fast, its deposition rate is somewhat less at around 1 μm $min^{-1}$ for the amorphous precursor. This gives an overall RCE-DR production rate which is around 50 times faster compared to CSD or PLD conductors.

## 5 Performance regimes and flux pinning

For most of the first quarter of a century since the discovery of HTS, all the focus was on optimising pinning at 65–77 K, the temperature range accessible to liquid nitrogen. In the last decade that focus has shifted to lower temperature operation. The reason is two-fold: firstly, the lack of ability to achieve adequate flux pinning at 77 K to attain the in-field performance required by applications and secondly, the developing capability to cool to 20 K or lower relatively easily using closed-cycle electrical cooling systems.

There exists a general relationship between the performance of the different processing methods, their supersaturation level, and their optimal operating regime (Fig. 5a). A clear trend line of negative slope shows the dominating influence of supersaturation, typically governing this correlation beyond the level of any engineered pinning present in these commercial conductors. Hence, higher supersaturation processes result in better high-field, low-temperature performance but worse low-field, high-temperature performance. Thus, the lower supersaturation processes (RCE-DR and CSD) are best suited to 77 K, self-field applications

(**REGION 1A**) while the highest supersaturation process (high rate PLD) is best suited to 4.2 K, high-field applications (**REGION 3**).

The moderate-to-high supersaturation processes show intermediate values of both the 77 K, self-field $J_c$ and the 4.2 K, high-field $J_c$, yielding their optimal performance in the moderate temperature and field regions (**REGION 2**). We note that engineering different artificial pinning centres into particular conductors will lead to a shift in a given process towards a higher region, but the overall trend remains. This explains the deviation of the PLD and MOCVD samples from the strict supersaturation sequence of Table 1. The PLD samples have no pinning additives while the MOCVD samples have strong pinning additives which make them artificially appear to have higher supersaturation compared to PLD. However, when comparing MOCVD and PLD of similar performance it is important to weigh up the advantages and disadvantages of each process, as previously described. We discuss more about applicable performance regimes and supersaturation levels next.

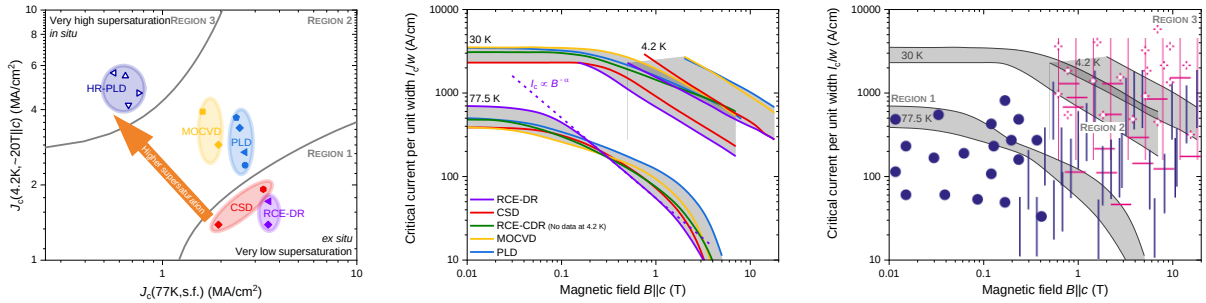


Fig. 5 | **Current-carrying performance metrics of commercial conductors in different temperature regimes. a** | $J_c$(4.2 K,~20 T) correlated with $J_c$(77 K,self-field) for different processing methods as well as the application regions to which they are best suited. Data taken from [69] and supplemented with data from panel b (diamond symbols) assuming a superconductor thickness of 2 µm. **b** | Magnetic field dependence of the critical current for three representative application temperatures, 77.5 K, 30 K and 4.2 K. Data sources: [70] (77.5 K, 30 K), [71] (4.2 K). **c** | Schematic of the effective flux pinning defect structures in each application region of temperature and magnetic field, against the range of commercial $I_c$ values at each representative application temperature transferred from panel b.

## 5.1 Conductor performance

The critical current per unit width of conductor ($I_c/w$) at the different representative temperatures of 4.2 K, 30 K and 77.5 K is plotted on Fig. 5b for a range of commercially-manufactured conductors available in long lengths from industrial suppliers, produced using each of the processing methods listed in Table 1. It is important to show commercial conductor performance because it represents a validated benchmark for a long conductor. Hence, the data shown is not intended to be necessarily the best conductor obtained using a particular process but is rather generally representative of differences between the different processes and typical for commercially marketed wires of the last three to five years. The actual suppliers of the wires featured are not stated as the purpose of the plot is not to compare the performance of conductors from different manufacturers, but rather to show what is possible across the different application regimes for a given processing method.

The performance data clearly demonstrates the trends noted earlier when relating the degree of supersaturation of the processing method to the $I_c$ for the different application regimes for the conductor. The optimal types of pinning defect for the different regimes are illustrated schematically in Fig. 5c. All regimes require nanometre spaced imperfections of nanometre dimension (even at zero applied field, since the self-field generated by the current-carrying conductor is already enough to produce flux lines having a sub-micrometre spacing). It is the subtleties of the sizes, distributions and combinations of the pinning defects that determine the pinning behaviour at any given temperature and field.[72] Currently, those commercial conductors that are pinning-enhanced have 3D (nanoparticle) and 1D (nanorod) pinning defects

intentionally engineered into them,[73] rather than the range of other defects, targeting 65–77 K performance enhancement.

### 5.1.1 Low-field, 77 K (REGION 1) performance

As already mentioned, by far the greatest effort to date has been expended by research groups and wire manufacturers alike on enhancing the 77 K low field performance of the conductors. In part, this is due to the simple accessibility of this regime for iterative testing, and in part to the persistent aspiration that this is the regime in which these high temperature superconductors should be utilised. Laboratory samples[74] have been demonstrated with critical current densities of up to 7 MA $cm^{-2}$ at 77 K while commercially mass-produced conductors can reach specified values of 4–5 MA $cm^{-2}$ in the best cases,[75] noting that there are good reasons why the current density in the thicker conductors required for application is diminished compared to very thin research samples.[76] For a long time, the depairing current of the REBCO material of around 30 MA $cm^{-2}$ at 77 K, zero field, was held up as a goal for these efforts but as further advancement stalled, it became clear that a lower limit resulting from a fundamental limitation on the possible strength of an idealised pinning site had already been reached, and represented the true performance limitation of the materials.[77] Further performance enhancement must rely on the development of thicker high-performance films or must focus on higher-field lower-temperature regimes where a gap between the present performance and the depinning critical current remains.

As we see from Fig. 5b, for the least favourable field direction, $B \| c$ (where no pinning resulting from the blocking layers along the *ab* planes of the crystal structure contributes to the performance), PLD is universally optimal across all regimes, except at the lowest fields (< 0.2 T, **REGION 1A**) where the low supersaturation, uniform RCE-DR process wins out. Above 0.2 T (**REGION 1B**), PLD is the best performing conductor, with the next best being MOCVD, then RCE-CDR, with CSD and RCE-DR following. While each conductor has not necessarily been optimised for its performance in this regime, all things being equal, that is if the same amount of artificial pinning centres were added to each conductor, this order is as expected based on the degree of supersaturation of Table 1. However, in this regime, very slight modifications to sample composition and processing conditions will yield large changes in the pinning behaviour, as the number and sizes of the pinning defects will be easily modified. From the point of view of tuning conductors for different applications requirements, this can be beneficial but in terms of controlling the process, it is challenging. The easiest method with which to achieve consistent, reproducible behaviour is PLD because the high supersaturation means a high density of columnar pinning centres, in addition to a highly reproducible REBCO microstructure.

As shown in Fig. 5c, all the way to the irreversibility field at around 7 T, strong correlated defects (1D nanorods) and weak random defects (3D nanoparticles) contribute to the pinning, with the nanoparticles being more effective at low fields and the nanorods being effective from there on. The optimal compositions of these artificial pinning centres have been researched for nearly 20 years, and a broad range of perovskites and rare earth oxides have been developed for this purpose.[78]

### 5.1.2 Mid-field, 30 K (REGION 2) performance

As the temperature is lowered to 30 K, the reduction in coherence length and reduced thermal fluctuations mean denser, smaller pinning centres are more effective for pinning with respect to their behaviour at 77 K.[79] The question is which pinning centres are optimal in this regime. This is a difficult region since a complex defect population comprising strong correlated defects along both *ab* and *c* directions, columnar grain boundaries, extended 1D nanorods, 0D defects and stacking faults all act together as effective pinning centres (Fig. 5c).[72] It is not yet clear exactly what balance of mixed pinning defects is optimal or indeed how to achieve that balance.[78]

PLD enables the most straightforward defect engineering of films, since it can easily be tuned with deposition temperature and rate to produce a wide range of pinning defect structures in a reproducible way.[50,80,81]

Fig. 5b shows that the vapour processed conductors produced by PLD, MOCVD and RCE-CDR all behave similarly at 30 K, although MOCVD exhibits a slightly improved performance across the intermediate field range from 0.1 T to 4 T. This may be because of a more optimised concentration of extended 1D nanorods. PLD, in contrast, because of its higher supersaturation growth and energetic deposition, will have a higher concentration of 0D pinning defects (i.e. more sub-nm disorder). The *ex situ* CSD and RCE-DR conductors have lower in-field performance than the *in situ* conductors discussed above. The post-deposition heat treatments for these processes typically result in both larger and less columnar pinning defects (although there has been significant progress at the laboratory scale in engineering-in very fine nanoparticle pinning centres[82] which are important for low-temperature, high-field pinning). CSD conductors retain moderate pinning in this region, likely because of the high density of stacking faults. For the RCE-DR conductors, pinning comes from a different source, likely a higher concentration of 0D defects arising from local disorder from the very rapid reaction. Overall, at 30 K, while there is good pinning from the non line-of-sight methods, in the absence of fine columnar grains and associated defects, it is ultimately less effective than that provided by the line-of-sight methods.

### 5.1.3 High-field, 4.2 K (REGION 3) performance

On Fig. 5c, we show that 0D defects play a more dominant role than mixed pinning defects at the lowest temperatures and highest fields. It is noted that to match flux densities of 10–30 T, the 0D defect spacing should be of the order of 8–15 nm.

Fig. 5b shows that at 4.2 K as at 30 K the *in situ* PLD and MOCVD conductors exhibit the best performance, accounted for by the secondary 0D defects arising from the dense columnar grains and extended 1D nanorods.[83] PLD slightly outperforms MOCVD, as is expected for the higher supersaturation, highly energetic process capable of producing more 0D defects.

Again similar to the case at 30 K, the non line-of-sight, lower supersaturation CSD and RCE-DR conductors have lower (by around a factor of two) in-field $I_c/w$ values than the line-of-sight PLD and MOCVD conductors. For RCE-DR, the decay of $I_c/w$ is slower than for CSD, whereas at 30 K it was similar. This is likely related to a higher concentration of 0D defects in RCE-DR arising from the very rapid reaction process. For CSD, different kinds and densities of 0D defects arise from strain fields around the edges of stacking faults which form during the growth process around 3D nanoparticle additions.[84] Hence, these are secondary-effect 0D defects.[78]

It is important to note that applications operating at 4.2 K can tolerate a much higher density of 0D defects, since at 4.2 K it doesn't matter if the critical temperature is substantially reduced as a result of disorder induced by the high concentration of defects. However, a very high density of defects can cause significant buckling of the superconducting CuO planes[85] which will impede supercurrent flow. Overall, there has been little work to date on controlled 0D defect engineering in combination with quantitative 0D defect concentration determination, and this is an important area for further work.

## 5.2 In-field behaviour

To learn more about the different mixed pinning mechanisms that are effective in the different application regimes, we explore the in-field behaviour of the commercial conductors in greater detail. Fig. 6 shows the trend in α value with temperature for the different processing methods for which complete data is available. α is the power-law exponent characterising the decay of the critical current with applied field, $I_c \propto B^{-\alpha}$, which as can be seen on the plots of Fig. 5b is broadly maintained between the low-field plateau (due to single-

vortex pinning and/or self-field effects) and the drop-off in $I_c$ towards zero on approaching the irreversibility field. We summarise in Table 2 the major contributing pinning defects for each method at low and high temperatures. Below, we discuss the behaviour observed either side of 40 K (being the approximate mid-range temperature, below which lie **REGIONS 2** and **3** and above which lies **REGION 1B**).

| | Effective at low temperatures | Effective across all temperatures | Effective at high temperatures |
|---|---|---|---|
| **CSD** | 3D nanoparticles, effective strain fields around 3D nanoparticles and 2D stacking faults | | |
| **RCE-DR** | 0D defects resulting from fast growth | | 3D nanoparticles |
| **MOCVD** | 0D defects associated with 1D nanorods | high density of 1D nanorods | |
| **PLD** | 0D defects | 1D dislocation lines along columnar 2D grain boundaries | |

Table 2 | **Defect species providing the most effective flux pinning in the different temperature regimes for the optimum performance coated conductors produced by the different processing methods of Fig. 5.**

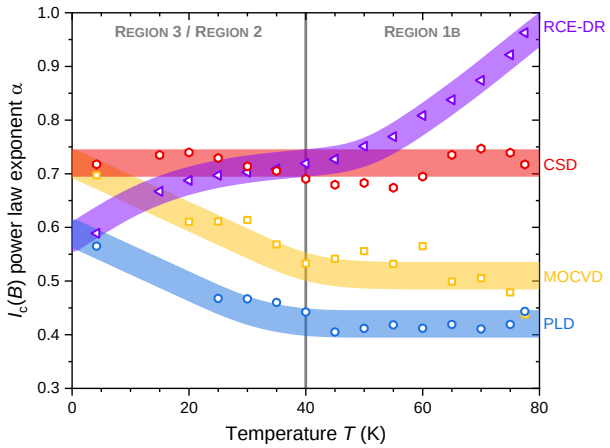


Fig. 6 | **In-field performance of commercial conductors in different temperature regimes.** Power law exponent (α) of the field decay of $I_c$ versus temperature for the different processing methods (except RCE-CDR where insufficient data is available). Values are extracted from the data shown in Fig. 5b, as well as additional data from the same source [70].

### 5.2.1 Low-temperature regime below 40 K (REGIONS 2 and 3)

The low temperature α value varies by a comparatively small amount across the processing methods, ranging between 0.55 and 0.75. We recall Fig. 5c which shows that 0D defect pinning and columnar defect pinning are both operative in this region, with the presence or absence of 0D defects becoming increasingly important towards the lower temperatures. Of course, both defects intrinsic to the processing route and artificial pinning additives play a role in determining α.[86] We note that a lower α value does not necessarily imply a higher $I_c$ because of the variable extent of the single-vortex pinning (plateau) region, as well as inherent variations in the self-field $I_c$ achieved by the particular processes. Hence, although MOCVD exhibits a higher α value than PLD, its $I_c$ remains similar (slightly higher at low fields and dropping off at high fields) due to an extended single-vortex pinning region.

Across the low temperature range from 4.2 K to 40 K, CSD exhibits the highest α value of just above 0.7, reflecting weak collective pinning originating from nanoscale strain fields around the nanoparticles and stacking faults present.[84] PLD produces the lowest low-temperature α value of around 0.55, consistent with pinning from 0D point defects arising from the high supersaturation growth. From 4.2 K to 40 K, its α value remains the lowest, decreasing to around 0.4–0.5. Dislocation lines along its highly columnar grain boundaries act as a linear array of strong columnar pinning centres,[87,88,89] around which the shearing of unpinned flux lines nucleated at the grain boundary by the increasing field leads to the observed α value.[69] The RCE-DR process yields a similar 4.2 K α value to PLD, consistent with 0D defect pinning resulting from the very fast growth process. By 40 K, the value has risen to around 0.7, similar to that for CSD and consistent with weak collective pinning. At 4.2 K, MOCVD has a similar α value to CSD, again indicative of weak collective pinning. There are fewer 0D defects present in MOCVD than PLD, likely because of the lower supersaturation

of the process. However, upon increasing temperature to 40 K, like PLD, the α value reduces for MOCVD as pinning from columnar defects takes over. RCE-DR and CSD don't have these columnar defects which means their α values do not decrease with increasing temperature.

### 5.2.2 High-temperature regime above 40 K (REGION 1B)

At higher temperatures, the pinning efficacy generally improves due to the existence of well-established effective pinning structures and the process optimisation steps that have served to encourage their formation, even in samples for which no artificial pinning centres have been introduced. Consequently, α typically drops. The notable exception is RCE-DR, for which α rises quite rapidly from its low-temperature value above 40 K. Hence, while RCE-DR has a lower α value than CSD at low temperatures, it is higher above about 60 K and reaches the vicinity of 1, reflecting pure collective pinning, around 77 K. We noted that there exists some measure of effective 0D pinning at low temperatures in RCE-DR; however, the pinning strength of such defects will not be sufficient to remain effective at the higher temperatures. The operative pinning defect structure is now 3D nanoparticles but using conventional processing their density is not high enough to effectively pin all the flux lines present in-field. That said, in laboratory-scale RCE-DR samples made with precise compositional tuning,[67] the films behave similarly to CSD samples at 77 K, demonstrating the possibility of achieving similarly effective defect structures at much higher growth rates. This reiterates the important influence of precise compositional tuning and process specifics on the pinning behaviour above 40 K, as noted previously in section 5.1.1.

The CSD process maintains a broadly constant α value of around 0.7 across the full temperature range. The pinning centres present, predominantly 3D nanoparticles and associated stacking faults and their strain fields are not as effective as others at low temperatures, but they maintain their effectiveness to high temperatures, likely as a result of the strain fields dominating at lower temperatures, transitioning to the stacking faults themselves dominating at higher temperatures.[90] Both MOCVD and PLD conductors exhibit an improvement in their already good low-temperature α value as the temperature is increased, dropping to around 0.5 and 0.4, respectively. These values reflect the extended 1D nanorods and/or columnar grain boundaries dominating at the higher temperatures. In the case of MOCVD we note, however, that for different conductors prepared using the same method, there exist wide variations in behaviour in the high-temperature region, including a complete reversal of the trends observed here. This again reinforces the fact that above 40 K, the precise form and density of columnar defects has a decisive influence on the pinning behaviour.[91]

In summary, for the measured contemporary commercial conductors the operative pinning mechanism is broadly the same from 4.2 K to 40 K, with a range of mechanisms, but the columnar microstructure of PLD conductors is particularly effective. Above 40 K, for all methods, there is great sensitivity of α to the precise balance of the different pinning defects. PLD produces the lowest α values over the widest temperature range. This is not to say, however, that the other methods can't be made to reproduce the low-α PLD behaviour across a wide temperature range, as has been closely achieved by MOCVD in some cases. More insight into this is given by recent results on laboratory-scale samples, as discussed next.

## 5.3 Best laboratory-scale performance data

We now consider recent progress in laboratory-scale samples synthesised by industry-proven methods. The critical current density, $J_c$, rather than $I_c$, is the performance metric used here because it shows what may be possible in terms of enhanced pinning and therefore in terms of performance enhancement for commercial conductors in the future.

We focus on performance enhancement at the temperatures of interest of 4.2 K and 30 K (Fig. 7a) where there is still strong scope for optimisation. We highlight key examples of the most significant advances

reported in recent times, comparing these laboratory results with the previously presented commercial wire $I_c$ ranges, shown as shaded regions on the plot. It is immediately apparent that recent laboratory-scale samples are able to outperform commercial wire at these temperatures quite significantly. Broadly speaking, laboratory-scale conductors perform at 30 K equivalent to the best commercial conductors at 4.2 K, with their performance at 4.2 K being correspondingly higher.

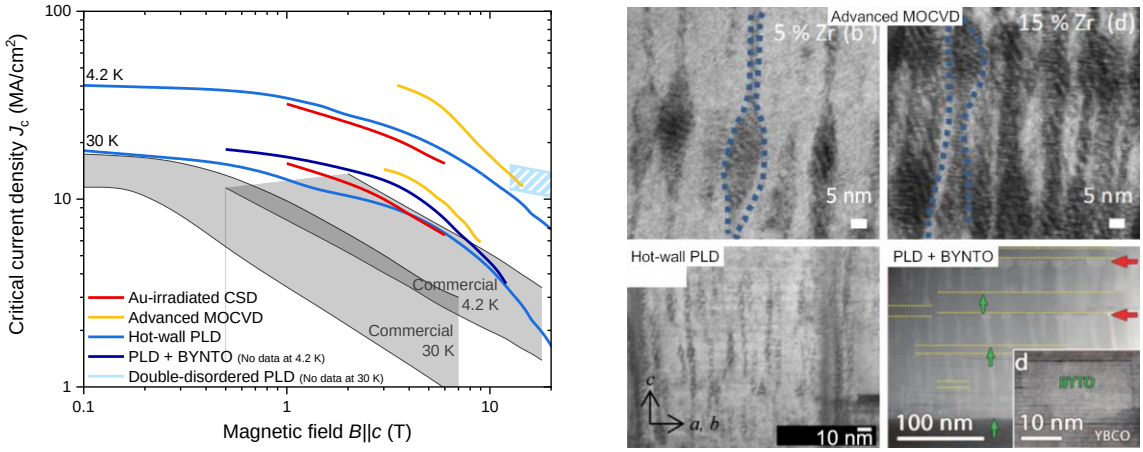


Fig. 7 | **Best laboratory-scale REBCO wire performance. a** | Comparison of various state-of-the-art laboratory techniques for producing high-performance conductors, compared with contemporary commercial conductor performance. Laboratory-scale samples broadly perform at 30 K equivalent to the best commercial wires at 4.2 K, albeit with a lower irreversibility field, whilst samples at 4.2 K exhibit a 3–5 times improvement over that. Data sources: Au-irradiated CSD [92]; Advanced MOCVD [93,94]; Hot-wall PLD [95]; PLD+BYNTO [96]; Double-disordered PLD [103]. **b** | Transmission electron microscopy examples of mixed dimensionality defects engineered into the REBCO layer of laboratory-scale samples through different deposition techniques. Images reproduced from [102,95,104] with permission.

### 5.3.1 Advanced metal-organic chemical vapour deposition

The first demonstration of strongly enhanced pinning at low temperatures in MOCVD samples was reported in 2014. Xu *et al.* showed[97] in MOCVD laboratory-scale samples on metal substrates that high volume fraction (15 mol.%) additions of Zr into REBCO yielded record performance (exceeding 10 MAcm$^{-2}$ at 4.2 K, 16 T||*c*). A complex mixed pinning microstructure of fine extended 1D $BaZrO_3$ nanorods with 25 nm spacing and 9 nm diameter were present as well as $RE_2O_3$ (3D) nanoparticles and planar (2D) stacking faults of CuO. At 4.2 K, the films had a high α value (close to 1) indicating pinning from a high density of weak 0D uncorrelated pins, but they also had a much enhanced $J_c$. From field angle dependent measurements of $J_c$ at 30 K in films with dense extended nanorods, isotropic behaviour was observed, consistent with the predominance of 0D pins.[98] The origin of these uncorrelated pinning centres is uncertain but is likely from secondary-effect point (0D) defects arising from the 2D and 3D defects, as well as from strain fields around the high-density 1D nanorods. The strain may give rise to 1D misfit dislocations[99] as well as to cation disorder.[100] Evidence for the possibility of cation disorder comes from measurements of highly extended *c* lattice parameters in Zr-added conductors.[93] The important role of dislocations for low-temperature pinning has also recently been considered[101] and warrants further detailed investigation for differently nanoengineered conductors.

More recent work[93,94] has demonstrated remarkable improvements in $J_c$ via this method (Fig. 7a). To understand what the optimum Zr doping level is and why, different amounts of Zr addition were studied. At 30 K, a lower Zr level of 5 mol.% gave a better $J_c$ for fields below 14 T, but the higher Zr level of 15 mol.% tended towards better performance above 14 T.[102] The microstructures in both cases were qualitatively similar (Fig. 7b, upper panels), i.e. long continuous nanorods as small as 3.5 nm diameter – close to the vortex diameter – passing through the entire film with 10 and 30 nm spacing for 15% and 5% doping, respectively, intersected by regular $RE_2O_3$ nanoparticles. For the 15% doping, there is possibly too much structural disorder (cation disorder and perturbation of the CuO planes) to achieve a good lower-field performance. We discuss

later how a mixed pinning microstructure might be optimised without compromising the microstructural integrity of the film.

### 5.3.2 Advanced pulsed laser deposition

Advanced PLD techniques show similar low-temperature performance enhancements to those seen in advanced MOCVD (Fig. 7a). The Fujikura company together with other researchers in Japan have shown excellent pinning at both 4.2 K and 30 K in laboratory-scale samples of REBCO with $BaHfO_3$ artificial pinning centres prepared using hot-wall PLD on metal substrates.[95] Hot-wall PLD likely enables more uniform heating and highly uniform columnar grains and hence an evenly-distributed high density of dislocations, explaining why Fujikura wires have some of the highest in-field $I_c$ values of any coated conductor even in the absence of artificial pinning centres.[42] With $BaHfO_3$ addition, a dense array of nanorods aligned with the *c*-axis is observed in the better-performing slower-grown samples (Fig. 7b, lower left panel). The performance results lie somewhat below the advanced MOCVD conductors, particularly at intermediate fields. The reports did not specify the amount of $BaHfO_3$ added to the films, but it appears from Fig. 7b that while fine (few nm diameter), dense (10 nm spaced) rods are obtained, the density of $RE_2O_3$ nanoparticles is lower than that present in the MOCVD samples. (This is because stoichiometric $BaHfO_3$ is added rather than elemental Zr as in the MOCVD case and so the REBCO matrix is not rendered $RE_2O_3$-rich by Ba consumption.)

Thus, the pinning microstructure for the hot-wall PLD sample is less complex than for MOCVD, although complex defect structures have been obtained by PLD in other reports. A notable example comes from the Bruker company (as-reported high field data only shown in Fig. 7a) who created fanning extended 1D nanorods of $BaZrO_3$, and certainly high levels of secondary 0D disorder along with this.[103] Consequently, the performance resulting from this complex "double-disordered" microstructure exceeds that of both the hot-wall PLD and the advanced MOCVD at high fields.

Another complex microstructure arises from double perovskites of the $Ba_2RE(Nb,Ta)O_6$ series, most typically $Ba_2Y(Nb,Ta)O_6$ (BYNTO).[96,104,105] Here, extended 1D nanorods with hammerhead spacer regions giving a 3D pinning structure are obtained (Fig. 7b, lower right panel) and excellent $J_c$ performance is achieved (Fig. 7a). While low temperature data has only so far been acquired for samples prepared on single crystal substrates, and hence is not directly comparable with that obtained for samples on technical substrates, there is strong potential as the BYNTO compositions have shown strong performance on technical substrates at 77K.[105]

### 5.3.3 Chemical solution deposition plus ion irradiation

As already discussed, the relatively low supersaturation of the CSD process means that achieving 0D defects is challenging. One way around this is to introduce columnar defects post-growth. This has been done successfully using gold ion irradiation in a reel-to-reel process,[92] giving rise to 5 nm diameter columnar defects, with performance at 4.2 K and 30 K similar to PLD (Fig. 7a). The results are highly promising, but it is unclear if the costs associated with the processing could ultimately produce commercially viable wire.[106] The direct introduction of point defects into coated conductor materials through proton irradiation has also been a subject of investigation, both for CSD[107] and RCE.[108]

### 5.3.4 Summary of approaches to pinning optimisation at low temperatures

Point defect engineering for optimising the high field, low temperature performance of REBCO is still at a relatively early stage of development. As already noted, 0D defects are most effectively engineered as secondary defects and hence they are not formed in a well-controlled manner. Also, the question of whether quasi-0D defects (very fine nanoparticles or nanoscale strain fields) are beneficial for high-field pinning at low temperatures remains uncertain.[78] At the same time, the evidence for enhanced pinning from true 0D defects has been questioned recently.[98] More work is needed on both the understanding of the nature of

point-like pinning and the means to controlled engineering of a high density of point-like defects. Whatever the means and whatever point-like defects are engineered, maintaining flat CuO planes, highly aligned grains and clean grain boundaries is also necessary to achieve the highest possible $J_c$, although these ideal microstructural features will inevitably be sacrificed somewhat to structural perturbations caused by the other-dimensional defects required to engender them.

# 6 Outlook

## 6.1 Future approaches for coated conductors

As far as pinning at 77 K goes (**REGIONS 1A and B**), a huge amount of work has already been done and conductors have been well optimised. At 30 K and 4.2 K (the critically important **REGIONS 2 and 3**), less work has been done and there is certainly room for more materials nano-engineering to further optimise performance. An optimised 4.2 K / 30 K conductor for high field applications would consist of a material having a mixed defect landscape, including defects of all dimensionalities ultimately leading to a high fraction of secondary-effect point-like defects processed as a thick conductor.[109] For widespread uptake, particularly for applications in **REGION 2**, this ideal defect landscape must be engineered-in by a method that is as low cost (and hence fast) as possible. While there has been a huge effort directed towards defect engineering in general, there has been less attention paid to developing fast, low-cost processing methods with high yield resulting from broad processing windows.

To meet both performance and cost requirements, it would be ideal to combine the performance benefits of a high supersaturation process such as PLD (which gives reliable and reproducible properties over long lengths in thick conductors and enables a wide range of pinning nanostructures and dimensionalities) with the cost benefits of a low supersaturation process. Looking again at Table 1, and moving down in supersaturation from PLD, but retaining a line-of-sight *in situ* process so that critically important extended 1D nanorods can easily be engineered, one might consider the moderate supersaturation processes. However, their lower supersaturation will always mean that process variability will be more challenging than it is for PLD. With PLD, the driving force for nucleation and columnar growth is very high, and the formation of unwanted and misaligned phases is much less probable even at large thicknesses. Possible modified approaches to the current processes to give higher supersaturation and higher speed include:

- A high supersaturation process with liquid added to speed the process.[61] Overall this would yield a moderate supersaturation process. Such a method is listed as high-rate PLD + liquid in Table 1. The high degree of supersaturation allows for the creation of a complex mixed pinning microstructure as well as higher speed of growth to minimise process cost.

- A moderate supersaturation process (MOCVD or RCE-CDR) with increased rare earth content to increase the supersaturation level. This could be achieved by using rare earth containing pinning centre additives. Increased supersaturation will facilitate growth over a wider range of processing conditions and enable more 0D defects to be formed, similar to high-rate PLD. For these moderate supersaturation processes, in order to grow thicker films while preventing unwanted phase formation or misorientation, the use of higher growth temperatures (or lower oxygen partial pressures) will ensure more perfect extended 1D defect formation.

- A low supersaturation process which is line-of-sight to enable stabilised columnar growth and extended 1D nanorods to be formed. This would be possible if RCE-DR and RCE-CDR were merged, combining the advantages of both the presence of liquid and the line-of-sight growth. Also, for the fast liquid-assisted processes, pinning centres which have relatively low melting points should be studied as these will be able to self-assemble more readily into columns during the rapid growth.

## 6.2 Emerging applications

Recently, several applications have arisen on the near-term horizon that depend critically on coated conductor technology for their viability, and that represent potential transformations both of their respective industries and of the superconductor industry itself. In contrast to the established range of applications of high-temperature superconductors summarised at the opening of this review, these emerging applications are unable to be realised using either low-temperature or BSCCO-based high-temperature superconductors. They therefore represent the genuinely new capabilities, rather than incremental opportunities, offered by this technology as it approaches maturity. Given their importance, it is also likely that once achieved, one of these may become the "killer application" that will drive volume production of coated conductors in the same way that MRI drove the production of low temperature superconductors, lowering costs to the point where the economic balance tips in favour of the more conventional applications also.

### 6.2.1 Compact fusion reactors for power generation

The prospect of man-made fusion power – harnessing the power of the sun here on Earth – is a game-changer in many respects. The provision of essentially limitless clean energy would allow humanity to break free from its reliance on the Earth's stored energy reserves of the last billion years, in any case now approaching depletion, and to continue its industrial and societal growth that is intimately dependent on its exponentially-increasing consumption of energy.

There are now several significant commercial enterprises striving to develop compact fusion reactors based on high-temperature superconductors.[110] There are two approaches to confining the fuel plasma sufficiently for fusion to occur: the first, adopted by the major publicly-funded $20bn international project ITER and its planned successor DEMO, is to increase the size of the reactor; while the second, newly possible with the advent of commercial-scale REBCO manufacture, is to increase the strength of the magnetic field. While the fusion power increases in proportion to the volume of the reactor, it varies as the magnetic field to the power four.[111] As a consequence, by doubling the field on the plasma from the roughly 5 T of ITER to roughly 10 T, the volume of the reactor can be reduced by more than an order of magnitude. Such "compact" fusion reactors are projected to be built by the mid-2020s and could potentially lead to operational power plants by 2030, before ITER itself is operational, and decades ahead of the ITER programme's plans for an operational power plant.[112]

The ITER magnets operate in liquid helium at 4.2 K. The most critical toroidal field coils must generate 5.3 T on the plasma and experience a maximum field on the windings of 11.8 T. Each of the 18 coils comprises 6.5 km of cable formed from 1000 strands of low-temperature superconducting $Nb_3Sn$ wire, for a total of more than 100,000 km produced by nine suppliers between 2008 and 2015, requiring the ramp-up of global production from 15 to 100 tonnes per year.[113] In contrast, the REBCO coils of proposed compact fusion devices would operate at 20 K and generate a field of 10 T on the plasma, being required to withstand fields on the windings in excess of 20 T, unachievable with other superconductors.[114] A commercial-scale compact fusion reactor would require 5–10,000 km of coated conductor, again representing several years of annual global production at current rates. Alternative designs take advantage of the higher operating temperatures of high-temperature superconductors to alter the geometry of the reactor, achieving the same size gains at fields similar to that of ITER, opening the potential to operate at even higher temperatures.[115] In this way, while large fusion reactors fall solidly within **REGION 3**, compact fusion reactors straddle **REGIONS 2 and 3**, and hence have the potential to utilise the **REGION 2** enhancements outlined in this work – enhancements from which they could greatly benefit.[116]

From the perspective of the compact fusion industry, REBCO has been described as an enabling technology the equivalent of the lightweight internal combustion engine for powered flight. From the perspective of the high-temperature superconductor industry, it is widely considered that fusion power may become the "MRI

of HTS," that is to say the killer application, unachievable through other means, that propels the technology out of the laboratory and into the world at large, breaking free of the chicken and egg situation of demand being limited by the high price, but price being inflated due to a lack of demand. A single commercial compact fusion reactor would require more HTS wire than the current annual production, and once a proven technology, demand for fusion reactors can be expected to far outstrip demand for MRI machines. This increased demand can in turn be expected to reduce production costs, opening up other areas of application that are presently cost-limited.

### 6.2.2 Electric aircraft motors and generators

Turning from supply to demand, the greatest global challenge of the 21st century is the abatement of climate change to which transportation is a major contributor. In particular, the aviation sector contributes 2–3% of total greenhouse gas emissions (rising to 5% of "radiative forcing", which accounts for the disproportionate effect of the emissions at altitude), the international component of which, crucially, is not even measured when assessing progress towards global emissions reduction targets due to the present intractability of the challenge.[117] Consequently this source has the potential to rise with ever-growing demand to become a quarter of the total carbon budget by 2050[118] as other sectors act to reduce their contribution to the total.

The development of electrically-powered aircraft to reduce emissions through increased efficiency in the first instance, and ultimately – when electrical energy storage systems of sufficient capacity, energy density and lifecycle reliability become feasible – to eliminate point-of-use emissions as so successfully done by the adoption of electrical technologies across other sectors hinges on the availability of an electric motor of sufficient power-to-weight ratio.[119] It is now broadly acknowledged that the necessary specification of 25 kW per kg (more than double the performance limit of conventional machines) can only be achieved through the adoption of superconducting technology,[120] and that only high-temperature superconductors can feasibly be operated at the temperatures achievable by an on-board cryogenics system.[121] In the hybrid turboelectric drivetrain proposed pending the development of adequate energy storage technology, a conventional fuel is burned to power a superconducting generator,[122] the output of which is then distributed between multiple superconducting electric motors.[123] This decoupling of the generator from the propeller allows both to operate independently at peak efficiency throughout the flight, increasing fuel efficiency (and reducing corresponding greenhouse gas emissions) by 30% and thereby largely counteracting the unchecked growth in aviation emissions since 1990, which has been double the rate of the rest of the economy. The adoption of distributed propulsion reduces both fuel consumption and engine noise, another significant area of concern.

### 6.2.3 Space-based applications

With the recent resurgence in space activity driven by the accelerating commercialisation of the space sector, a number of potential applications of high-temperature superconductors in space are being reconsidered in light of the considerable technological advancement in the field.[124] These range from enhanced benefit re-applications of terrestrial devices such as superconducting magnetic energy storage systems,[125] superconducting levitating bearings[126] and research magnets[127] to entirely new, uniquely space-based applications such as radiation shields to protect humans from solar and cosmic radiation during interplanetary space voyages or within extra-terrestrial habitats[128] and novel electrically-powered motion systems such as superconducting helicon[129] and magnetoplasmadynamic thrusters[130] and magnetorquers.[131] All of these potential applications notwithstanding, reports of superconductors that have operated in space are vanishingly sparse. The high temperature superconductivity space experiment (HTSSE) launched a number of cryocooled small-scale electronic devices on the ARGOS satellite in 1999.[132] In terms of large-scale devices, a small low-temperature superconducting magnet powered the adiabatic demagnetisation refrigerator of the soft x-ray spectrometer on the Hitomi satellite launched in 2016 but lost shortly

thereafter.[133] The detector of the alpha magnetic spectrometer (AMS-02) was originally designed, built and tested to operate using a low-temperature superconducting magnet[134] but this was ultimately replaced with a permanent magnet prior to launch to extend the runtime beyond that achievable using liquid helium as a coolant.[135] The next-generation instrument, AMS-100, has a proposed design incorporating an HTS magnet formed from coated conductors, but is yet to be built.[136] To date, no wire-based superconducting technology has been reportedly deployed on a space mission. However, the coming decade is likely to see a rapid expansion of development work targeting this area[137] as the new application areas outlined above are further developed through proof-of-concept to prototype, accompanied by the ongoing adaptation and optimisation of ground-based cryocoolers for the space environment.[138] In this way, the application of high temperature superconducting coated conductors promises to assist humanity in transcending the final frontier.

### 6.2.4 Cable designs

To build practical devices from our conductors, many additional engineering aspects need to be taken into consideration. Primary among these for ac applications is the need to limit the ac losses that are non-zero even for superconducting materials. Since many applications require more current than can be conveyed by a single conductor, there is a need to parallel conductors together to form a cable, and in this case it is necessary both for the reduction of ac losses and to ensure equal current sharing between conductors to transpose them along the length of the cable. Methods of achieving this include Roebel cabling or conductor on round core technologies, which simultaneously aim to resolve the issue of the hard-to-work-with high aspect ratio tape geometry of the conductors.[139] Furthermore, conductor striation can be used to emulate the fine filaments of low temperature superconductors.[140]

A second issue of critical importance to application is the mechanical strength of the conductor, ensuring that it can support the substantial stresses induced by the magnetic pressure without elongation (which reduces $I_c$) or delamination of any of the complex stack of thin film layers.[141] Characterisation of conductors in this respect is at an early stage. Strengthening is through the use of different substrate materials or lamination with a high-strength material.

Finally, adequate stabilisation of the superconductor in the geometry of the stack is a challenge exacerbated by the poor quench propagation characteristics of HTS, which lead to the formation of localised hotspots that are difficult to detect or mitigate before catastrophic failure occurs. The thermal isolation of the superconductor layer from the substrate by the insulating buffer layers is one aspect of the problem that could be overcome by the development of conducting buffer layers,[142] but in the meantime, a one-sided stabilisation by a metallic capping layer is commonly utilised, unfortunately increasing the overall cross-section of the superconductor and thereby reducing its $J_e$. No-insulation coils, whereby turn-to-turn decoupling of the conductor is achieved simply through the higher resistance of the metallic layer, which provides improved thermal equalisation and thereby stability, are a promising but as-yet unproven approach to addressing this issue.[143]

## 6.3 Summary

The field of applied high temperature superconductivity has come a long way in the last 30 years, inventing and realising an amazing coated conductor and cabling technology that can and should be used on a large scale across a wide range of power and magnet applications. The low energy consumption of HTS is critical for a sustainable future and can be applied in multiple energy areas, all the way from generation to transmission to storage and ultimately consumption. Most recently, the fusion area has come to the fore, with compact Tokamak reactors being critically reliant on the use of coated conductor technology to achieve functionality. By comparing the many different conductor processing methods being used by industry today in terms of their degree of supersaturation, it is possible to understand and explain how and why the resulting

conductors behave as they do, over the wide range of temperatures and magnetic fields required by the different applications. The application regime of 20–40 K, above 1 T (termed **REGION 2** in this paper) is highlighted as the most important one for the majority of proposed HTS applications. A complex mixed pinning landscape is required to achieve the goal of high performance in this region and it is still early days in terms of its optimisation, its emergence as a distinct entity having been learned only from the failure of 77 K performance optimisation to achieve similar enhancements at 40 K and below. More effort needs to be focused on understanding and optimising the wide-ranging and interacting defect structures at lower temperatures where performance falls short of application requirements. All the while, lower cost, more efficient and highly reliable processing methods must continue to be developed as today's coated conductor remains too expensive for widespread uptake and effective competition with conventional alternatives. Overall, a large effort needs to be maintained in novel materials design, engineering and processing to bring the labours of the past 30 years to fruition.

## Acknowledgements

The authors gratefully acknowledge T. Bedford for background research contributing to this work, S. H. Moon for a critical reading of the manuscript, and M. W. Rupich, J. Hänisch, A. Palau, G. Brittles and A. K. Kursumovic for helpful points of discussion.

J.L.M.-D. acknowledges funding from the Royal Academy of Engineering, Grant CiET1819_24, the Harding Foundation, and Leverhulme Trust Grant RPG-2020-041.

## Author contributions

The authors jointly contributed to the collation and writing of all parts of this review.

## Competing interests

The authors declare no competing interests.

## References

[1] Bednorz, J. G. and Müller, K. A. Possible high Tc superconductivity in the Ba–La–Cu–O system. Z. Phys. B 64, 189 (1986).

[2] Wu, M. K., Ashburn, J. R., Torng, C. J., Hor, P. H., Meng, R. L., Gao, L., Huang, Z. J., Wang, Y. Q. & Chu, C. W. Superconductivity at 93 K in a new mixed-phase Y-Ba-Cu-O compound system at ambient pressure. *Phys. Rev. Lett.* **58**, 908 (1987).

[3] Schilling, A., Cantoni, M., Guo, J. D. & Ott, H. R. Superconductivity above 130 K in the Hg–Ba–Ca–Cu–O system. *Nature* **363**, 56 (1993).

[4] Scanlan, R. M., Malozemoff, A. P. & Larbalestier, D. C. Superconducting materials for large scale applications. *Proc. IEEE* **92**, 1639 (2004).

[5] Kobayashi, S. Development and Manufacture of Bi-2223 Wires in Research, Fabrication and Applications of Bi-2223 HTS Wires. Sato, K. (ed.) World Scientific Series in Applications of Superconductivity and Related Phenomena. pp. 137-150. ISBN 978-981-4749-25-1. doi:10.1142/9789814749268_0010 (2016).

[6] Wimbush, S. C., Strickland, N. M. & Long, N. J. Low-temperature scaling of the critical current in 1G HTS wires. *IEEE Trans. Appl. Supercond.* **25**, 6400105 (2015).

[7] Hashi, K., Ohki, S., Matsumoto, S., Nishijima, G., Goto, A., Deguchi, K., Yamada, K., Noguchi, T., Sakai, S., Takahashi, M., Yanagisawa, Y., Iguchi, S., Yamazaki, T., Maeda, H., Tanaka, R., Nemoto, T., Suematsu, H., Miki, T., Saito, K. & Shimizu, T. Achievement of 1020 MHz NMR. *J. Magn. Reson.* **256**, 30 (2015).

[8] Shen, T., Bosque, E., Davis, D., Jiang, J., White, M., Zhang, K., Higley, H., Turqueti, M., Huang, Y., Miao, H., Trociewitz, U., Hellstrom, E., Parrell, J., Hunt, A., Gourlay, S., Prestemon S. & Larbalestier, D. Stable, predictable and training-free operation of superconducting Bi-2212 Rutherford cable racetrack coils at the wire current density of 1000 A/mm$^2$. *Sci. Rep.* **9**, 10170 (2019).

[9] Noguchi, S., Park, D., Choi, Y., Lee, J., Li, Y., Michael, P. C., Bascuñán, J., Hahn, S. & Iwasa, Y. Quench analyses of the MIT 1.3-GHz LTS/HTS NMR magnet. *IEEE Trans. Appl. Supercond.* **29**, 4301005 (2019).

[10] Yoon, S., Kim, J., Cheon, K., Lee, H., Hahn, S. & Moon, S.-H. 26 T 35 mm all-$GdBa_2Cu_3O_{7-x}$ multi-width no-insulation superconducting magnet. *Supercond. Sci. Technol.* **29**, 04LT04 (2016).

[11] Hahn, S., Kim, K., Kim, K., Hu, X., Painter, T., Dixon, I., Kim, S., Bhattarai, K. R., Noguchi, S., Jaroszynski, J. & Larbalestier, D. C. 45.5-tesla direct-current magnetic field generated with a high-temperature superconducting magnet. *Nature* **570**, 496 (2019).

[12] Fazilleau, P., Chaud, X., Debray, F., Lécrevisse, T. & Song, J.-B. 38 mm diameter cold bore metal-as-insulation HTS insert reached 32.5 T in a background magnetic field generated by resistive magnet. *Cryogenics* **106**, 103053 (2020).

[13] Bai, H., Abraimov, D. V., Boebinger, G. S., Bird, M. D., Cooley, L. D., Dixon, I. R., Kim, K. L., Larbalestier, D. C., Marshall, W. S., Trociewitz, U. P. & Weijers, H. W. The 40 T superconducting magnet project at the National High Magnetic Field Laboratory. *IEEE Trans. Appl. Supercond.* **30**, 8970538 (2020).

[14] Liu, J., Wang, Q., Qin, L., Zhou, B., Wang, K., Wang, Y., Wang, L., Zhang, Z., Dai, Y., Liu, H., Hu, X., Wang, H., Cui, C., Wang, D., Wang, H., Sun, J., Sun, W. & Xiong, L. World record 32.35 tesla direct-current magnetic field generated with an all-superconducting magnet. *Supercond. Sci. Technol.* **33**, 03LT01 (2020).

[15] Computer History Museum, The silicon engine: a timeline of semiconductors in computers. Available at https://www.computerhistory.org/siliconengine/timeline/.

[16] Grant, P. M. & Sheahen, T. P. Cost projections for high temperature superconductors. Presented at: Applied Superconductivity Conference, Desert Springs, CA, USA, 13–18 September 1998. *arXiv:cond-mat/0202386* (2002).

[17] Rey, C. (ed.) Superconductors in the power grid: materials and applications. Woodhead Publishing. ISBN 978-1-78242-029-3 (2015).

[18] Wimbush, S. C. Superconductors, in "Materials for sustainable energy applications: conversion, storage, transmission, and consumption," X. Moya and D. Muñoz-Rojas (eds.), Pan Stanford Publishing, Singapore, ISBN 978-9-814-41181-3 (2016).

[19] Marchionini, B. G., Yamada, Y., Martini, L. & Ohsaki, H. High-temperature superconductivity: a roadmap for electric power sector applications, 2015–2030. *IEEE Trans. Appl. Supercond.* **27**, 0500907 (2017).

[20] Tosaka, T., Miyazaki, H., Iwai, S., Otani, Y., Takahashi, M., Tasaki, K., Nomura, S., Kurusu, T., Ueda, H., Noguchi, S., Ishiyama, A., Urayama, S. & Fukuyama, H. Project overview of HTS magnet for ultra-high-field MRI system. *Physics Procedia* **65**, 217 (2015).

[21] Takayama, S., Koyanagi, K., Miyazaki, H., Takami, S., Orikasa, T., Ishii, Y., Kurusu, T., Iwata, Y., Noda, K., Obana, T., Suzuki, K., Ogitsu, T. & Amemiya, N. Design and test results of superconducting magnet for heavy-ion rotating gantry. *J. Phys.: Conf. Ser.* **871**, 012083 (2017).

[22] Godeke, A., Alberty, L., Akcöltekin, E., Babouche, R., Detourbe, C., Nast, R., Radermacher, Ch., Röcken, H., Roth, A., Schillo, M., vom Stein, P., Walpole, M., Wittschen, J., Hayashi, K., Shizuya, E., Krooshoop, H. J. G., Lubkemann, R., Nijhuis, A., Vermeer, C. H., Wessel, W. A. J., Krause, J., Wiezoreck, J., Otto, A. & Saraco, L. Research at Varian on applied superconductivity for proton therapy. *Supercond. Sci. Technol.* **33**, 064001 (2020).

[23] Song, J. B., Choi, Y. H., Yang, D. G., Kim, Y. G., Kim, K. L. & Lee, H. G. Review of core technologies for development of 2G HTS NMR/MRI magnet: a status report of progress in Korea University. *Results Phys.* **7**, 3264 (2017).

[24] Wang, X., Gourlay, S. A. & Prestemon, S. O. Dipole magnets above 20 tesla: research needs for a path via high-temperature superconducting REBCO conductors. *Instruments* **3**, 62 (2019).

[25] Choi, J., Kim, T., Lee, C.-K., Jeon, D.-S., Park, G.-W., Cho, S., Park, M., Yu, I.-K. & Iwakuma, M. Commercial design and operating characteristics of a 300 kW superconducting induction heater (SIH) based on HTS magnets. *IEEE Trans. Appl. Supercond.* **29**, 3700105 (2019).

[26] Sohn, M.-H., Kim, S., Sim, K., Bae, J.-H., Lee, S.-J. & Park, H.-Y. Fabrication and characteristics of 2G HTS current leads. *IEEE Trans. Appl. Supercond.* **20**, 1755 (2010).

[27] Schreiner, F., Gutheil, B., Noe, M., Reiser, W., Huwer, S., Hanebeck, C., Räch, C., Röhrenbeck, M. & Schreiner, F. Design and manufacturing of a multistage cooled current lead for superconducting high current DC busbars in industrial applications. *IEEE Trans. Appl. Supercond.* **27**, 4802405 (2017).

[28] Radebaugh, R. Cryocoolers: the state of the art and recent developments. *J. Phys.: Condens. Matter* **21**, 164219 (2009).

[29] Ter Brake, H. J. M. & Wiegerinck, G. F. M. Low-power cryocooler survey. *Cryogenics* **42**, 705-718 (2002).

[30] Iijima, Y., Tanabe, N., Kohno, O. & Ikeno, Y. In-plane aligned $YBa_2Cu_3O_{7-x}$ thin films deposited on polycrystalline metallic substrates. *Appl. Phys. Lett.* **60**, 769 (1992).

[31] Goyal, A., Parans Paranthaman, M. & Schoop, U. The RABiTS approach: using rolling-assisted biaxially textured substrates for high-performance YBCO superconductors. *MRS Bull.* **29**, 552 (2004).

[32] Arendt, P. N. & Foltyn, S. R. Biaxially textured IBAD-MgO templates for YBCO-coated conductors. *MRS Bull.* **29**, 543 (2004).

[33] Usoskin, A., Betz, U., Dietrich, R. & Schlenga, K. Long HTS coated conductor processed via large-area PLD/ABAD for high-field applications. *IEEE Trans. Appl. Supercond.* **26**, 6602304 (2016).

[34] Prusseit, W., Nemetschek, R., Hoffmann, C., Sigl, G., Lümkemann, A. & Kinder, H. ISD process development for coated conductors. *Physica C* **426-431**, 866 (2005).

[35] Selvamanickam, V., Chen, Y., Xiong, X., Xie, Y., Zhang, X., Rar, A., Martchevskii, M., Schmidt, R., Lenseth, K. & Herrin, J. Progress in second-generation HTS wire development and manufacturing. *Physica C* **468**, 1504 (2008).

[36] Schoop, U., Rupich, M. W., Thieme, C., Verebelyi, D. T., Zhang, W., Li, X., Kodenkandath, T., Nguyen, N., Siegal, E., Civale, L., Holesinger, T., Maiorov, B., Goyal, A. & Paranthaman, M. Second generation HTS wire based on RABiTS substrates and MOD YBCO. *IEEE Trans. Appl. Supercond.* **15**, 2611 (2005).

[37] Feenstra, R., Wojtyniak, B., Kunert, J., Bennewitz, J., Falter, M., Rikel, M. & Baecker, M. Development of cost-effective chemical solution deposition YBCO superconductor tapes. Presented at Coated Conductors for Applications 2016, September 11-14, 2016, Aspen, Colorado, USA. Available at https://nationalmaglab.org/images/magnet_development/asc/searchable_docs/asc_resources/coated_conductors/2016/co_06_feenstra.pdf. Accessed 1 July 2020.

[38] Dinner, R. B., Moler, K. A., Beasley, M. R. & Feldmann, D. M. Enhanced current flow through meandering grain boundaries in YBa2Cu3O7−δ films. *Appl. Phys. Lett.* **90**, 212501 (2007).

[39] Sundaram, A., Zhang, Y., Knoll, A. R., Abraimov, D., Brownsey, P., Kasahara, M., Carota, G. M., Nakasaki, R., Cameron, J. B., Schwab, G., Hope, L. V., Schmidt, R. M., Kuraseko, H., Fukushima, T. & D Hazelton, D. W. 2G HTS wires made on 30 µm thick Hastelloy substrate. *Supercond. Sci. Technol.* **29**, 104007 (2016).

[40] Kar, S., Luo, W. & Selvamanickam, V. Ultra-small diameter round REBCO wire with robust mechanical properties. *IEEE Trans. Appl. Supercond.* **27**, 6603204 (2017).

[41] Moon, S. H. SuNAM developed new process named RCE-DR: the practical highest throughput process. Presented at The European Conference on Applied Superconductivity EUCAS 2013, September 15-19 2013, Genova, Italy. Available at https://snf.ieeecsc.org/sites/ieeecsc.org/files/documents/snf/abstracts/moon_0.pdf. Accessed 1 July 2020.

[42] Kakimoto, K., Igarashi, M., Hanada, Y., Hayashida, T., Tashita, C., Morita, K., Hanyu, S., Sutoh, Y., Kutami, H., Iijima, Y. & Saitoh, T. High-speed deposition of high-quality RE123 films by a PLD system with hot-wall heating. *Supercond. Sci. Technol.* **23**, 014016 (2010).

[43] Watanabe, T., Kuriki, R., Iwai, H., Muroga, T., Miyata, S., Ibi, A., Yamada, Y. & Shiohara, Y. High rate deposition by PLD of YBCO films for coated conductors. *IEEE Trans. Appl. Supercond.* **15**, 2566 (2005).

[44] Selvamanickam, V., Xie, Y., Reeves J. & Chen, Y. MOCVD-based YBCO-coated conductors. *MRS Bull.* **29**, 579 (2004).

[45] Matias, V., Rowley, E. J., Coulter, Y., Maiorov, B., Holesinger, T., Yung, C., Glyantsev, V. & Moeckly, B. YBCO films grown by reactive co-evaporation on simplified IBAD-MgO coated conductor templates. *Supercond. Sci. Technol.* **23**, 014018 (2010).

[46] Matias, V., Hänisch, J., Reagor, D., Rowley, E. J. & Sheehan, C. Reactive co-evaporation of YBCO as a low-cost process for fabricating coated conductors. *IEEE Trans. Appl. Supercond.* **19**, 3172 (2009).

[47] Holesinger, T. G., Civale, L., Maiorov, B., Feldmann, D. M., Coulter, J. Y., Miller, D. J., Maroni, V. A., Chen, Z., Larbalestier, D. C., Feenstra, R., Li, X., Huang, Y., Kodenkandath, T., Zhang, W., Rupich, M. W. & Malozemoff, A. P. Progress in nanoengineered microstructures for tunable high-current, high-temperature superconducting wires. *Adv. Mater.* **20**, 391 (2008).

[48] Kim, H.-S., Oh, S.-S., Ha, H.-S., Youm, D., Moon, S.-H., Kim, J. H., Dou, S. X., Heo, Y.-U., Wee, S.-H. & Goyal, A. Ultra-high performance, high-temperature superconducting wires via cost-effective, scalable, co-evaporation process. *Sci. Rep.* **4**, 4744 (2015).

[49] Qi, X. & MacManus-Driscoll, J. L. Liquid phase epitaxy processing for high temperature superconductor tapes. *Curr. Opin. Solid State Mater. Sci.* **5**, 291 (2001).

[50] Harrington, S. A., Durrell, J. H., Wang, H., Wimbush, S. C., Tsai, C. F. & MacManus-Driscoll, J. L. Understanding nanoparticle self-assembly for a strong improvement in functionality in thin film nanocomposites. *Nanotechnology* **21**, 095604 (2010).

[51] Zhao, R., Li, W., Lee, J. H., Choi, E. M., Liang, Y., Zhang, W., Tang, R., Wang, H., Jia, Q., MacManus-Driscoll, J. L. & Yang, H. Precise tuning of $(YBa_2Cu_3O_{7-\delta})_{1-x}$:$(BaZrO_3)_x$ thin film nanocomposite structures. Adv. Func. Mater. **24**, 5240 (2014).

[52] Guo, H., Sun, D., Wang, W., Gai, Z., Kravchenko, I., Shao, J., Jiang, L., Ward, T. Z., Snijders, P. C., Yin, L., Shen, J. & Xu, X. Growth diagram of $La_{0.7}Sr_{0.3}MnO_3$ thin films using pulsed laser deposition. *J. Appl. Phys.* **113**, 234301 (2013).

[53] Thornton, J. A. High rate thick film growth. *Ann. Rev. Mater. Sci.* **7**, 239 (1977).

[54] Capper, P., Irvine, S. & Joyce, T. Epitaxial Crystal Growth: Methods and Materials. Fig. 14.1. In: Kasap, S. & Capper, P. (eds) Springer Handbook of Electronic and Photonic Materials. Springer, Cham. ISBN 978-3-319-48933-9 (2017).

[55] Christen, H. M. & Eres, G. Recent advances in pulsed-laser deposition of complex oxides. *J. Phys.: Condens. Matter* **20**, 264005 (2008).

[56] Díaz, A., Mechin, L., Berghuis, P. & Evetts, J. E. Evidence for vortex pinning by dislocations in $YBa_2Cu_3O_{7-\delta}$ low-angle grain boundaries. *Phys. Rev. Lett.* **80**, 3855 (1998).

[57] Chisholm, M. F. C. & Smith, D. A. Low-angle tilt grain boundaries in $YBa_2Cu_3O_7$ superconductors. *Phil. Mag. A* **59**, 181 (1989).

[58] Dimon, D., Chaudhari, P., Mannhart, J. & LeGoues, F. K. Orientation dependence of grain-boundary critical currents in $YBa_2Cu_3O_{7-\delta}$ bicrystals. *Phys. Rev. Lett.* **61**, 219 (1988).

[59] Khan, M. Z., Zhao, Y., Wu, X., Malmivirta, M., Huhtinen, H. & Paturi, P. (2018). Improved interface growth and enhanced flux pinning in YBCO films deposited on an advanced IBAD-MgO based template. *Physica C* **545**, 50 (2018).

[60] Foltyn, S. R., Tiwari, P., Dye, R. C., Le, M. Q. & Wu, X. D. Pulsed laser deposition of thick $YBa_2Cu_3O_{7-\delta}$ films with $J_c \geq 1$ MA/cm$^2$. *Appl. Phys. Lett.* **63**, 1848 (1993).

[61] Feighan, J. P. F., Lai, M. H., Kursumovic, A., Zhang, D., Wang, H., Moon, S. & MacManus Driscoll, J. L. Strong pinning at high growth rates in rare earth barium cuprate (REBCO) superconductor films grown with liquid-assisted processing (LAP) during pulsed laser deposition. Submitted (2020).

[62] Feldmann, D. M., Holesinger, T. G., Feenstra, R., Cantoni, C., Zhang, W., Rupich, M., Li, X., Durrell, J. H., Gurevich, A. & Larbalestier, D. C. Mechanisms for enhanced supercurrent across meandered grain boundaries in high temperature superconductors. *J. Appl. Phys.* **102**, 083912 (2007).

[63] Lee, J.-H., Lee, H., Lee, J.-W., Choi, S.-M., Yoo, S.-I. & Moon, S.-H. RCE-DR, a novel process for coated conductor fabrication with high performance. *Supercond. Sci. Technol.* **27** 044018 (2014).

[64] Ikeda, S., Motoki, T., Gondo, S., Nakamura, S., Honda, G., Nagaishi, T., Doi, T. & Shimoyama, J., Synthesis of thick YBCO films up to 3.0 μm on metallic substrates by a fluorine-free metal organic decomposition method. *Supercond. Sci. Technol.* **32**, 115003 (2019).

[65] Pop, C., Villarejo, B., Pino, F., Mundet, B., Ricart, S., de Palau, M., Puig, T. & Obradors, X. Growth of all-chemical high critical current $YBa_2Cu_3O_{7-\delta}$ thick films and coated conductors. *Supercond. Sci. Technol.* **32**, 015004 (2019).

[66] Soler, L., Jareño, J., Banchewski, J., Rasi, S., Chamorro, N., Guzman, R., Yáñez, R., Mocuta, C., Ricart, S., Farjas, J., Roura-Grabulosa, P., Obradors, X. & Puig, T. Ultrafast transient liquid assisted growth of high current density superconducting films. *Nature Comm.* **11**, 344 (2020).

[67] MacManus-Driscoll, J. L., Bianchetti, M., Kursumovic, A., Kim, G., Jo, W., Wang, H., Lee, J. H., Hong, G. W. & Moon, S. H. Strong pinning in very fast grown reactive co-evaporated $GdBa_2Cu_3O_7$ coated conductors. *APL Mater.* **2**, 086103 (2014).

[68] Yoshizumi, M., Nakanishi, T., Matsuda, J., Nakaoka, K., Sutoh, Y., Izumi, T. & Shiohara, Y. Crystal growth of YBCO coated conductors by TFA–MOD method. *Physica C* **468**, 1531-1533 (2008).

[69] Senatore, C., Barth, C., Bonura, M., Kulich, M. & Mondonico, G. Field and temperature scaling of the critical current density in commercial REBCO coated conductors. *Supercond. Sci. Technol.* **29**, 014002 (2016).

[70] Wimbush, S. & Strickland, N. A high-temperature superconducting (HTS) wire critical current database. figshare. Collection. doi:10.6084/m9.figshare.c.2861821.v10.

[71] Tsuchiya, K., Kikuchi, A., Terashima, A., Norimoto, K., Uchida, M., Tawada, M., Masuzawa, M., Ohuchi, N., Wang, X., Takao, T. & Fujita, S. Critical current measurement of commercial REBCO conductors at 4.2 K. *Cryogenics* **85**, 1 (2017).

[72] Jha, A. K. & Matsumoto, K. Superconductive REBCO thin films and their nanocomposites: the role of rare-earth oxides in promoting sustainable energy. *Front. Phys.* **7**, 82 (2019).

[73] Yoshida, Y., Miura, S., Tsuchiya, Y., Ichino, Y., Awaji, S., Matsumoto, K. & Ichinose, A. Approaches in controllable generation of artificial pinning center in $REBa_2Cu_3O_y$-coated conductor for high-flux pinning. *Supercond. Sci. Technol.* **30**, 104002 (2017).

[74] Foltyn, S. R., Civale, L., MacManus-Driscoll, J. L., Jia, Q. X., Maiorov, B., Wang, H. & Maley, M. Materials science challenges for high-temperature superconducting wire. *Nat. Mater.* **6**, 631–642 (2007).

[75] Published maximum wire specification of 150 A/4mm for 1 μm thick SuperPower wire (available at http://www.superpower-inc.com/system/files/SP_2G+Wire+Spec+Sheet_2014_web_v1.pdf, accessed 1 July 2020) and 180 A/4mm for 1.2 μm thick AMSC wire (available at https://www.amsc.com/wp-content/uploads/BRSAMP8700_DS_A4_0514_WEB.pdf, accessed 1 July 2020).

[76] Wimbush, S. C., Li, M., Vickers, M. E., Maiorov, B., Feldmann, D. M., Jia, Q. X. & MacManus-Driscoll, J. L. Interfacial strain-induced oxygen disorder as the cause of enhanced critical current density in superconducting thin films. *Adv. Func. Mater.* **19**, 835 (2009).

[77] Matsushita, T. & Kiuchi, M. Theoretical estimation of the upper limit of critical current density by flux pinning in superconductors under the influence of kinetic energy. *Appl. Phys. Express* **12**, 023004 (2019).

[78] Feighan, J. P. F., Kursumovic, A. & MacManus-Driscoll, J. L. Materials design for artificial pinning centres in superconductor PLD coated conductors. *Supercond. Sci. Technol.* **30**, 123001 (2017).

[79] Strickland, N. M., Wimbush, S. C., Kennedy, J. V., Ridgway, M. C., Talantsev, E. F. & Long, N. J. Effective low-temperature flux pinning by Au ion irradiation in HTS coated conductors. *IEEE Trans. Appl. Supercond.* **25**, 6600905 (2015).

[80] Wu, J. & Shi, J. Interactive modeling-synthesis-characterization approach towards controllable in situ self-assembly of artificial pinning centers in RE-123 films. *Supercond. Sci. Technol.* **30**, 103002 (2017).

[81] Miura, S., Yoshida, Y., Ichino, Y., Tsuruta, A., Matsumoto, K., Ichinose, A. & Awaji, S. Vortex pinning at low temperature under high magnetic field in $SmBa_2Cu_3O_y$ superconducting films with high number density and small size of $BaHfO_3$ nano-rods. *Supercond. Sci. Technol.* **28**, 114006 (2015).

[82] Li, Z., Coll, M., Mundet, B., Chamorro, N., Vallès, F., Palau, A., Gazquez, J., Ricart, S., Puig, T. & Obradors, X. Control of nanostructure and pinning properties in solution deposited $YBa_2Cu_3O_{7-x}$ nanocomposites with preformed perovskite nanoparticles. *Sci. Rep.* **9**, 5828 (2019).

[83] Braccini, V., Xu, A., Jaroszynski, J., Xin, Y., Larbalestier, D. C., Chen, Y., Carota, G., Dackow, J., Kesgin, I., Yao, Y., Guevara, A., Shi, T. & Selvamanickam, V. Properties of recent IBAD-MOCVD coated conductors relevant to their high field, low temperature magnet use. *Supercond. Sci. Technol.* **24**, 035001 (2011).

[84] Palau, A., Vallès, F., Rouco, V., Coll, M., Li, Z., Pop, C., Mundet, B., Gàzquez, J., Guzman, R., Gutierrez, J., Obradors, X. & Puig, T. Disentangling vortex pinning landscape in chemical solution deposited superconducting $YBa_2Cu_3O_{7-x}$ films and nanocomposites. *Supercond. Sci. Technol.* **31**, 034004 (2018).

[85] Ercolano, G., Bianchetti, M., Sahonta, S.-L., Kursumovic, A., Lee, J. H., Wang, H. & MacManus-Driscoll, J. L. Strong correlated pinning at high growth rates in $YBa_2Cu_3O_{7-x}$ thin films with $Ba_2YNbO_6$ additions. *J. Appl. Phys.* **116**, 033915 (2014).

[86] Maiorov, B., Baily, S. A., Zhou, H., Ugurlu, O., Kennison, J. A., Dowden, P. C., Holesinger, T. G., Foltyn, S. R. & Civale, L. Synergetic combination of different types of defect to optimize pinning landscape using $BaZrO_3$-doped $YBa_2Cu_3O_7$. *Nature Mater.* **8**, 398 (2009).

[87] L. Fernández, L., Holzapfel, B., Schindler, F., de Boer, B., Attenberger, A., Hänisch, J. & Schultz, L. Influence of the grain boundary network on the critical current of $YBa_2Cu_3O_7$ films grown on biaxially textured metallic substrates. *Phys. Rev. B* **67**, 052503 (2003).

[88] Palau, A., Puig, T., Gutierrez, J., Obradors, X. & de la Cruz, F. Pinning regimes of grain boundary vortices in $YBa_2Cu_3O_{7-x}$ coated conductors. *Phys. Rev. B* **73**, 132508 (2006).

[89] Stafford, B. H., Sieger, M., Ottolinger, R., Meledin, A., Strickland, N. M., Wimbush, S. C., Van Tendeloo, G., Hühne, R. & Schultz, L. Tilted $BaHfO_3$ nanorod artificial pinning centres in REBCO films on inclined substrate deposited-MgO coated conductor templates. *Supercond. Sci. Technol.* **30**, 055002 (2017).

[90] Puichaud, A.-H., Wimbush, S. C. & Knibbe, R. Enhanced low-temperature critical current by reduction of stacking faults in REBCO coated conductors. *Supercond. Sci. Technol.* **30**, 074005 (2017).

[91] Francis, A., Abraimov, D., Viouchkov, Y., Su, Y., Kametani, F. & Larbalestier, D. C. Development of general expressions for the temperature and magnetic field dependence of the critical current density in coated conductors with variable properties. *Supercond. Sci. Technol.* **33**, 044011 (2020).

[92] Rupich, M. W., Sathyamurthy, S., Fleshler, S., Li, Q., Solovyov, V., Ozaki, T., Welp, U., Kwok, W.-K., Leroux, M., Koshelev, A. E., Miller, D. J., Kihlstrom, K., Civale, L., Eley, S. & Kayani, A. Engineered pinning landscapes for enhanced 2G coil wire. *IEEE Trans. Appl. Supercond.* **26**, 6601904 (2016).

[93] Majkic, G., Pratap, R., Xu, A., Galstyan, E. & Selvamanickam, V. Over 15 MA/cm$^2$ of critical current density in 4.8 μm thick, Zr-doped (Gd,Y)$Ba_2Cu_3O_x$ superconductor at 30 K, 3T. *Sci. Rep.* **8**, 6982 (2018).

[94] Majkic, G., Pratap, R., Xu, A., Galstyan, E., Higley, H. C., Prestemon, S. O., Wang, X., Abraimov, D., Jaroszynski, J. & Selvamanickam, V. Engineering current density over 5kAmm$^{-2}$ at 4.2K, 14T in thick film REBCO tapes. *Supercond. Sci. Technol.* **31**, 10LT01 (2018).

[95] Fujita, S., Muto, S., Hirata, W., Yoshida, T., Kakimoto, K., Iijima, Y., Daibo, M., Kiss, T., Okada, T. & Awaji, S. Flux-pinning properties of $BaHfO_3$-doped EuBCO-coated conductors fabricated by hot-wall PLD. *IEEE Trans. Appl. Supercond.* **29**, 8001505 (2019).

[96] Rizzo, F., Augieri, A., Kursumovic, A., Bianchetti, M., Opherden, L., Sieger, M., Hühne, R., Hänisch, J., Meledin, A., Van Tendeloo, G., MacManus-Driscoll, J. L. & G. Celentano, G. Pushing the limits of applicability of REBCO coated conductor films through fine chemical tuning and nanoengineering of inclusions. *Nanoscale* **10**, 8187-8195 (2018).

[97] Xu, A., Delgado, L., Khatri, N., Liu, Y., Selvamanickam, V., Abraimov, D., Jaroszynski, J., Kametani, F. & Larbalestier, D. C. Strongly enhanced vortex pinning from 4 to 77 K in magnetic fields up to 31 T in 15 mol.% Zr-added (Gd, Y)-Ba-Cu-O superconducting tapes. *APL Materials* **2**, 046111 (2014).

[98] Yamasaki, H. Origin of collapse of $J_c(\theta)$ peaks at $H//c$ in low temperatures in (RE)BCO thin films with nanorods. *Supercond. Sci. Technol.* **32**, 09LT01 (2019).

[99] MacManus-Driscoll, J. L., Zerrer, P., Wang, H., Yang, H., Yoon, J., Fouchet, A., Yu, R., Blamire, M. G. & Jia, Q. X. Strain control and spontaneous phase ordering in vertical nanocomposite heteroepitaxial thin films. *Nature Mater.* **7**, 314 (2008).

[100] MacManus-Driscoll, J. L., Wells, M. P., Yun, C., Lee, J.-W., Eom, C.-B. & Schlom, D. G. New approaches for achieving more perfect transition metal oxide thin films. *APL Mater.* **8**, 040904 (2020).

[101] Khan, M. Z., Zhao, Y., Wu, X., Jha, R., Awana, V. P. S., Huhtinen, H. & Paturi, P. Improving the flux pinning with artificial BCO nanodots and correlated dislocations in YBCO films grown on IBAD-MgO based template. *IEEE Trans. Appl. Supercond.* **29**, 8002105 (2019).

[102] Galstyan, E., Pratap, R., Majkic, G., Kochat, M., Mohan, V. & Selvamanickam, V. Correlation between microstructure and in-field performance of Zr-added REBCO coated conductors made by advanced MOCVD. *IEEE Trans. Appl. Supercond.* **29**, 8001206 (2019).

[103] Usoskin, A., Betz, U., Hofacker, F., Rutt, A., Schlenga, K., Prause, B., Rossi, L., Bottura, L., Ballarino, A., Senatore, C., Kario, A., Goldacker, W., Meledin, A., Abraimov, D. & Larbalestier, D. Double-disordered HTS-coated conductors and their assemblies aimed for ultra-high fields: large area tapes. *IEEE Trans. Appl. Supercond.* **28**, 6602506 (2018).

[104] Rizzo, F., Augieri, A., Armenio, A. A., Galluzzi, V., Mancini, A., Pinto, V., Rufoloni, A., Vannozzi, A., Bianchetti, M., Kursumovic, A., MacManus-Driscoll, J. L., Meledin, A., Van Tendeloo, G. & Celentano, G. Enhanced 77 K vortex-pinning in $YBa_2Cu_3O_{7-x}$ films with $Ba_2YTaO_6$ and mixed $Ba_2YTaO_6$ + $Ba_2YNbO_6$ nano-columnar inclusions with irreversibility field to 11 T. *APL Materials* **4**, 061101 (2016).

[105] Sieger, M., Pahlke, P., Lao, M., Eisterer, M., Meledin, A., Van Tendeloo, G., Ottolinger, R., Hanisch, J., Holzapfel, B., Usoskin, A., Kursumovic, A., MacManus-Driscoll, J. L., Stafford, B. H., Bauer, M., Nielsch, K., Schultz, L. & Huhne, R. Tailoring microstructure and superconducting properties in thick $BaHfO_3$ and $Ba_2Y(Nb/Ta)O_6$ doped YBCO films on technical templates. *IEEE Trans. Appl. Supercond.* **27**, 6601407 (2017).

[106] Leroux, M., Kihlstrom, K. J., Holleis, S., Rupich, M. W., Sathyamurthy, S., Fleshler, S., Sheng, H. P., Miller, D. J., Eley, S., Civale, L., Kayani, A., Niraula, P. M., Welp, U. & Kwok, W.-K. Rapid doubling of the critical current of $YBa_2Cu_3O_{7-\delta}$ coated conductors for viable high-speed industrial processing. *Appl. Phys. Lett.* **107**, 192601 (2015).

[107] Jia, Y., LeRoux, M., Miller, D. J., Wen, J. G., Kwok, W. K., Welp, U., Rupich, M. W., Li, X., Sathyamurthy, S., Fleshler, S., Malozemoff, A. P., Kayani, A., Ayala-Valenzuela, O. & Civale, L. Doubling the critical current density of high temperature superconducting coated conductors through proton irradiation. *Appl. Phys. Lett.* **103**, 122601 (2013).

[108] Choi, W. J., Ahmad, D., Seo, Y. I., Ko, R. K. & Kwon, Y. S. Effect of the proton irradiation on the thermally activated flux flow in superconducting SmBCO coated conductors. *Sci. Rep.* **10**, 2017 (2020).

[109] Kwok, W.-K., Welp, U., Glatz, A., Koshelev, A. E., Kihlstrom, K. J. & Crabtree, G. W. Vortices in high-performance high-temperature superconductors. *Rep. Prog. Phys.* **79**, 116501 (2016).

[110] Kramer, D. Will doubling magnetic field strength halve the time to fusion energy? *Phys. Today* **71**, 25 (2018).

[111] Zohm, H. On the size of tokamak fusion power plants. *Phil. Trans. R. Soc. A* **377**, 20170437 (2019).

[112] Minervini, J. V. A pathway to fusion energy based on high-field REBCO superconducting magnets. Presented at WAMHTS-5, Budapest, April 11-12, 2019. Available at https://indico.cern.ch/event/775529/contributions/3309887/attachments/1828600/2993908/Minervini_HTS-for-Fusion-WAMHTS-5.pdf. Accessed 1 July 2020.

[113] Devred, A., Backbier, I., Bessette, D., Bevillard, G., Gardner, M., Jong, C., Lillaz, F., Mitchell, N., Romano, G. & Vostner, A. Challenges and status of ITER conductor production. *Supercond. Sci. Technol.* **27**, 044001 (2014).

[114] Uglietti, D., Bykovsky, N., Wesche,R. & Bruzzone, P. Development of HTS conductors for fusion magnets. *IEEE Trans. Appl. Supercond.* **25**, 4202106 (2015).

[115] Sykes, A., Costley, A. E., Windsor, C. G., Asunta, O., Brittles, G., Buxton, P., Chuyanov, V., Connor, J. W., Gryaznevich, M. P., Huang, B., Hugill, J., Kukushkin, A., Kingham, D., Langtry, A. V., McNamara, S., Morgan, J. G., Noonan, P., Ross, J. S. H., Shevchenko, V., Slade, R. & Smith, G. Compact fusion energy based on the spherical tokamak. *Nucl. Fusion* **58**, 016039 (2018).

[116] Bruzzone, P., Fietz, W. H., Minervini, J. V., Novikov, M., Yanagi, N., Zhai, Y. & Zheng, J. High temperature superconductors for fusion magnets. *Nucl. Fusion* **58**, 103001 (2018).

[117] Owen, B., Lee, D. S. & Lim, L. Flying into the future: aviation emissions scenarios to 2050. *Environ. Sci. Technol.* **44**, 2255 (2010).

[118] Pidcock, R. & Yeo, S. Analysis: Aviation could consume a quarter of 1.5C carbon budget by 2050. *Carbon Brief International Policy*, 8 August 2016. Available from https://www.carbonbrief.org/aviation-consume-quarter-carbon-budget. Accessed 1 July 2020.

[119] Luongo, C. A., Masson, P. J., Nam, T., Mavris, D., Kim, H. D., Brown, G. V., Waters, M. & Hall, D. Next generation more-electric aircraft: a potential application for HTS superconductors. *IEEE Trans. Appl. Supercond.* **19**, 1055 (2009).

[120] Ashcraft, S. W., Padron, A. S., Pascioni, K. A., Stout, Jr., G. W. & Huff, D. L. Review of propulsion technologies for N+3 subsonic vehicle concepts. NASA Technical Report TM—2011-217239 (2011). Available from https://ntrs.nasa.gov/archive/nasa/casi.ntrs.nasa.gov/20110022435.pdf. Accessed 1 July 2020.

[121] Haran, K. S., Kalsi, S., Arndt, T., Karmaker, H., Badcock, R., Buckley, B., Haugan, T., Izumi, M., Loder, D., Bray, J. W., Masson, P. & Stautner, E. W. High power density superconducting rotating machines—development status and technology roadmap. *Supercond. Sci. Technol.* **30**, 123002 (2017).

[122] Filipenko, M., Kühn, L., Gleixner, T., Thummet, M., Lessmann, M., Möller, D., Böhm, M., Schröter, A., Häse, K., Grundmann, J., Wilke, M., Frank, M., van Hasselt, P., Richter, J., Herranz-Garcia, M., Weidermann, C., Spangolo, A. & Klöpzig, M. Concept design of a high power superconducting generator for future hybrid-electric aircraft. *Supercond. Sci. Technol.* **33**, 054002 (2020).

[123] Berg, F., Palmer, J., Miller, P., Husband, M. & Dodds, G. HTS electrical system for a distributed propulsion aircraft. *IEEE Trans. Appl. Supercond.* **25**, 5202705 (2015).

[124] Mitschang, G. W. Space applications and implications of high temperature superconductivity. *IEEE Trans. Appl. Supercond.* **5**, 69 (1995).

[125] Evans, M. E. & Ignatiev, A. Lunar superconducting magnetic energy storage (LSMES). *NASA Report JSC-E-DAA-TN60059* (2018). Available at: https://ntrs.nasa.gov/archive/nasa/casi.ntrs.nasa.gov/20190001255. pdf. Accessed 1 July 2020.

[126] Angel, R., Worden, S. P., Borra, E. F., Eisenstein, D. J., Foing, B., Hickson, P., Josset, J.-L., Ma, K. B., Seddiki, O., Sivanandam, S., Thibault, S. & van Susante, P. A cryogenic liquid-mirror telescope on the moon to study the early universe. *Astrophys. J.* **680**, 1582Y1594 (2008).

[127] Dam, M., Battiston, R., Burger, W. J., Carpentiero, R., Chesta, E., Iuppa, R., de Rijk, G. & Rossi, L. Conceptual design of a high temperature superconducting magnet for a particle physics experiment in space. *Supercond. Sci. Technol.* **33**, 044012 (2020).

[128] Ambroglini, F., Battiston, R. & Burger, W. J. Evaluation of superconducting magnet shield configurations for long duration manned space missions. *Front. Oncol.* **6**, 97 (2016).

[129] Vitucci, J. J. Development and test of a superconducting helicon plasma thruster. *PhD thesis.* University of Maryland (2019). Available at: https://drum.lib.umd.edu/handle/1903/25159. Accessed 1 July, 2020.

[130] Glowacki, J., Badcock, R. & Long, N. Design analysis of an applied-field magnetoplasmadynamic thruster with superconducting magnet. *AIAA Propulsion and Energy 2019 Forum*, AIAA 2019-4081, doi:10.2514/6.2019-4081 (2019).

[131] Gettliffe, G. V., Porter, A. & Wesenberg, R. MAGESTIC: Magnetically enabled structures using interacting coils - NIAC Phase II Final Report. *NASA Innovative Advanced Concepts* (2015).

[132] Nisenoff, M. & Meyers, W. J. On-orbit status of the high temperature superconductivity space experiment. *IEEE Trans. Appl. Supercond.* **11**, 799 (2001).

[133] Shirron, P. J., Kimball, M. O., James, B. L., Muench, T., DiPirro, M. J., Letmate, R. V., Sampson, M. A., Bialas, T. G., Sneiderman, G. A., Porter, F. S. & Kelley, R. L. Operating modes and cooling capabilities of the 3-stage ADR developed for the soft-X-ray spectrometer instrument on astro-H. *Cryogenics* **74**, 2 (2016).

[134] Blau, B., Harrison, S. M., Hofer, H., Horvath, I. L., Milward, S. R., Ross, J. S. H., Ting, S. C. C., Ulbricht, J. & Viertel, G. The superconducting magnet system of AMS-02 – a particle physics detector to be operated on the International Space Station. *IEEE Trans. Appl. Supercond.* **12**, 349 (2002).

[135] Lübelsmeyer, K., Schultz von Dratzig, A., Wlochal, M., Ambrosi, G., Azzarello, P., Battistone, R., Becker, R., Becker, U., Bertucci, B., Bollweg, K., Burger, J. D., Cadoux, F., Cai, X. D., Capell, M., Choutko, V., Durantie, M., Gargiulo, C., Guandalini, C., Haino, S., Ionicae, M., Koulemzine, A., Kounine, A., Koutsenko, V., Laurenti, G.,

Lebedev, A., Martin, T., Oliva, A., Paniccia, M., Perrin, E., Rapin, D., Rozhkov, A., Schael, St., Tholen, H., Ting, S. C. C. & Zuccon, P. Upgrade of the Alpha Magnetic Spectrometer (AMS-02) for long term operation on the International Space Station (ISS). *Nucl. Instrum. Methods Phys. Res. A* **654**, 639 (2011).

[136] Schael, S., Atanasyan, A., Berdugo, J., Bretz, T., Czupalla, M., Dachwald, B., von Doetinchem, P., Duranti, M., Gast, H., Karpinski, W., Kirn, T., Lübelsmeyer, K., Maña, C., Marrocchesi, P. S., Mertsch, P., Moskalenko, I. V., Schervan, T., Schluse, M., Schröder, K.-U., Schultz von Dratzig, A., Senatore, C., Spies, L., Wakely, S. P., Wlochal, M., Uglietti, D. & Zimmermann, J. AMS-100: The next generation magnetic spectrometer in space – An international science platform for physics and astrophysics at Lagrange point 2. *Nucl. Instrum. Methods Phys. Res. A* **944**, 162561 (2019).

[137] Musenich, R., Adriani, O., Baudouy, B., Calvelli, V., Farinon, S., Papini, P. & Bertucci, B. A Proposal for a Superconducting Space Magnet for an Antimatter Spectrometer. *IEEE Trans. Appl. Supercond.* **30**, 4500305 (2020).

[138] Narasaki, K., Tsunematsu, S., Ootsuka, K., Kanao, K., Okabayashi, A., Mitsuda, K., Murakami, H., Nakagawa, T., Kikuchi, K., Sato, R., Sugita, H., Sato, Y., Murakami, M. & Kobayashi, M. Lifetime test and heritage on orbit of coolers for space use. *Cryogenics* **52**, 188 (2012).

[139] Uglietti, D. A review of commercial high temperature superconducting materials for large magnets: from wires and tapes to cables and conductors. *Supercond. Sci. Technol.* **32**, 053001 (2019).

[140] Vojenčiak, M., Kario, A., Ringsdorf, B., Nast, R., Van Der Laan, D. C., Scheiter, J., Jung, A., Runtsch, B., Gömöry, F. & Goldacker, W. Magnetization ac loss reduction in HTS CORC® cables made of striated coated conductors. *Supercond. Sci. Technol.* **28**, 104006 (2015).

[141] Barth, C., Mondonico, G. & Senatore, C. Electro-mechanical properties of REBCO coated conductors from various industrial manufacturers at 77 K, self-field and 4.2 K, 19 T. *Supercond. Sci. Technol.* **28**, 045011 (2015).

[142] Doi, T., Morimura, T., Horii, S. & Ichinose, A. High critical current density $YBa_2Cu_3O_7$ coating on conductive Nb-doped $SrTiO_3$ and Ni double-buffered {100}<001> textured pure Cu tape for low-cost coated conductors without generation of any insulative oxides at interfaces. *Appl. Phys. Express* **12**, 023010 (2019).

[143] Hahn, S., Kim, K., Kim, K., Lee, H. & Iwasa, Y. Current status of and challenges for no-insulation HTS winding technique. *J. Cryo. Super. Soc. Jpn.* **53**, 2 (2018).

## Figure 1 references

[1] Bednorz, J. G. & Müller, K. A. Possible high $T_c$ superconductivity in the Ba-La-Cu-O system. *Z. Phys. B* **64**, 189 (1986).

[2] Wu, M. K., Ashburn, J. R., Torng, C. J., Hor, P. H., Meng, R. L., Gao, L., Huang, Z. J., Wang, Y. Q. & Chu, C. W. Superconductivity at 93 K in a new mixed-phase Y-Ba-Cu-O compound system at ambient pressure. *Phys. Rev. Lett.* **58**, 908 (1987).

[3] Maeda, H., Tanaka, Y., Fukutomi, M. & Asano, T. A new high-$T_c$ oxide superconductor without a rare earth element. *Jpn. J. Appl. Phys.* **27**, L209 (1988).

[4] Iijima, Y., Tanabe, N., Kohno, O. & Ikeno, Y. In-plane aligned $YBa_2Cu_3O_{7-x}$ thin films deposited on polycrystalline metallic substrates, *Appl. Phys. Lett.* **60**, 769 (1992).

[5] Goyal, A., Norton, D. P., Budai, J. D., Paranthaman, M., Specht, E. D., Kroeger, D. M., Christen, D. K., He, Q., Saffian, B., List, F. A., Lee, D. F., Martin, P. M., Klabunde, C. E., Hartfield, E. & Sikka, V. K. High critical current

density superconducting tapes by epitaxial deposition of $YBa_2Cu_3O_x$ thick films on biaxially textured metals, *Appl. Phys. Lett.* **69**, 1795 (1996).

[6] Wang, C. P., Do, K. B., Beasley, M. R., Geballe, T. H. & Hammond, R. H. Deposition of in-plane textured MgO on amorphous $Si_3N_4$ substrates by ion-beam-assisted deposition and comparisons with ion-beam-assisted deposited yttria-stabilized-zirconia. *Appl. Phys. Lett.* **71**, 2955 (1997).

[7] MacManus-Driscoll, J. L., Foltyn, S. R., Jia, Q. X., Wang, H., Serquis, A., Civale, L., Maiorov, B., Hawley, M. E., Maley, M. P. & Peterson, D. E. Strongly enhanced current densities in superconducting coated conductors of $YBa_2Cu_3O_{7-x}$ + $BaZrO_3$. *Nature Materials* **3**, 439 (2004).

[8] Iwakuma, M., Tomioka, A., Konno, M., Hase, Y., Satou, T., Iijima, Y., Saitoh, T., Yamada, Y.,Izumi, T. & Shiohara, Y. Development of a 15 kW motor with a fixed YBCO superconducting field winding. *IEEE Trans. Appl. Supercond.* **17**, 1607 (2007).

[9] Fair, R., Lewis, C., Eugene, J. & Ingles, M. Development of an HTS hydroelectric power generator for the Hirschaid power station. *J. Phys.: Conf. Ser.* **234**, 032008 (2010).

[10] Applied Materials press release. Applied Materials receives order for two transmission-class superconducting fault current limiters. April 14, 2015. Available at: http://www.appliedmaterials.com/company/news/press-releases/2015/04/applied-materials-receives-order-for-two-transmission-class-superconducting-fault-current-limiters. Accessed 1 July 2020.

[11] Gupta, R., Anerella, M., Joshi, P., Higgins, J., Lalitha, S., Sampson, W., Schmalzle, J. & Wanderer, P. Design, construction, and testing of a large-aperture high-field HTS SMES coil. *IEEE Trans. Appl. Supercond.* **26**, 5700208 (2016).

[12] Glasson, N., Staines, M., Allpress, N., Pannu, M., Tanchon, J., Pardo, E., Badcock, R. & Buckley, R. Test results and conclusions from a 1 MVA superconducting transformer featuring 2G HTS Roebel cable. *IEEE Trans. Appl. Supercond.* **27**, 5500205 (2017).

[13] Parkinson, B. J., Bouloukakis, K. & Slade, R. A. A compact 3 T all HTS cryogen-free MRI system. *Supercond. Sci. Technol.* **30**, 125009 (2017).

[14] Kovalev, I. A., Surin, M. I., Naumov, A. V., Novikov, M. S., Novikov, S. I., Ilin, A. A., Polyakov, A. V., Scherbakov, V. I. & Shutova, D. I. Test results of 12/18 kA ReBCO coated conductor current leads. *Cryogenics* **85**, 71 (2017).

[15] Choi, J., Kim, T., Lee, C.-K., Jeon, D.-S., Park, G.-W., Cho, S., Park, M., Yu, I.-K. & Iwakuma, M. Commercial design and operating characteristics of a 300 kW superconducting induction heater (SIH) based on HTS magnets. *IEEE Trans. Appl. Supercond.* **29**, 3700105 (2019).

[16] Bergen, A., Andersen, R., Bauer, M., Boy, H., ter Brake, M., Brutsaert, P., Bührer, C., Dhallé, M., Hansen, J., ten Kate, H., Kellers, J., Krause, J., Krooshoop, E., Kruse, C., Kylling, H., Pilas, M., Pütz, H., Rebsdorf, A., Reckhard, M., Seitz, E., Springer, H., Song, X., Tzabar, N., Wessel, S., Wiezoreck, J., Winkler, T. & Yagotyntsev, K. Design and in-field testing of the world's first ReBCO rotor for a 3.6 MW wind generator. *Supercond. Sci. Technol.* **32**, 125006 (2019).

[17] Kim, J., Kim, Y., Yoon, S., Shin, K., Lee, J., Jung, J. S., Lee, J. T., Kim, J.-G., Kim, D., Yoo, J., Lee, H., Moon, S.-H. & Hahn, S. Design, construction, and operation of an 18 T 70 mm no-insulation (RE)$Ba_2Cu_3O_{7-x}$ magnet for an axion haloscope experiment. *Rev. Sci. Instrum.* **91**, 023314 (2020).

[18] Lee, C., Son, H., Won, Y., Kim, Y., Ryu, C., Park, M. & Iwakuma, M. Progress of the first commercial project of high-temperature superconducting cables by KEPCO in Korea. *Supercond. Sci. Technol.* **33**, 044006 (2020).